***Journal of Iberian Geology* 41 (2) 2015:** 183-204
http://dx.doi.org/10.5209/rev_JIGE.2015.v41.n2.46696

www.ucm.es/info/estratig/journal.htm
ISSN (print): 1698-6180. ISSN (online): 1886-7995

Journal of Iberian Geology
AN INTERNATIONAL PUBLICATION OF EARTH SCIENCES

Phreatomagmatic activity and associated hydrothermal processes in the lamproitic volcano of Cancarix (Southeast Spain)

M. Reolid*, I. Abad, M. Sánchez-Gómez

Departamento de Geología and CEACT, Universidad de Jaén, Campus Las Lagunillas, 23071 Jaén, Spain.

*e-mail addresses: mreolid@ujaen.es (M.R., *Corresponding author); miabad@ujaen.es (I.A.); msgomez@ujaen.es (M.S.-G.)*

Received: 22 March 2014 / Accepted: 22 November 2014 / Available online: 20 July 2015

Abstract

The study of the Cancarix volcano structure (Sierra de las Cabras, SE Spain) and the regional observations in similar lamproite volcanoes suggest that these magmas were emplaced during the Miocene in relation to transtensive structures at the North end of the Betic Cordillera. These structures were able to reactivate previous basement faults which facilitated the ascending circulation of enriched ultrapotassic magma. Two episodes are distinguished: 1) explosive volcanism due to the interaction between magma and groundwater from the karstic system of the host carbonate rocks, which generated a phreatomagmatic-effusive complex and 2) volcanic-building with crystal-rich magma. The phreatomagmatic breccia distribution is conditioned by the tectonic structure of the host rock, with maximum thickness over the marls basement, mechanically less competent, which is controlling the preferential magma movement towards the S-SE. Chemical, mineralogical and textural study of the host rocks and the volcanic products indicates that following the magmatic activity hydrothermal processes ocurred, with: (1) the genesis of new minerals (namely, saponitic smectite and serpentine minerals) in the host rock clasts from the phreatomagmatic breccia; and (2) the recrystallisation of dolomite and amorphous silica growing up to 20 m from the contact in porous carbonates. In contrast, marls and micritic carbonates show no recrystallisation, only a slight enrichment of Mg and some exotic elements, limited to the first few metres.

Keywords: phreatomagmatic-effusive complex, hydrothermal alteration, saponite, SE Spain Volcanic Province

Resumen

El estudio de la estructura del Volcán de Cancarix (Sierra de las Cabras, SE España) y las observaciones regionales en volcanes lamproíticos similares sugieren que el emplazamiento de los magmas tuvo lugar durante el Mioceno en relación con estructuras transtensivas en el extremo Norte de la Cordillera Bética. Estas estructuras favorecieron la reactivación de fallas previas del basamento que facilitaron la circulación ascendente de magmas enriquecidos en Mg y K. Se han diferenciado dos episodios de emisión de material en el Volcán de Cancarix: 1) vulcanismo explosivo debido a la interacción del magma con el agua subterránea procedente del sistema kárstico de los carbonatos que componen la roca caja, que generó un complejo freatomagmático (brechas y lavas) y 2) una etapa de vulcanismo efusivo con un magma rico en cristales que dio lugar al domo lamproítico. La distribución de la brecha freatomagmática estuvo condicionada por la estructura tectónica de la roca caja, con un máximo espesor sobre las margas, mecánicamente menos competentes. En consecuencia, la dirección preferente de avance del magma fue hacia el S-SE, donde las margas son predominantes. El estudio geoquímico, mineralógico y textural de la roca caja y del material volcánico indica que tras la actividad volcánica, hubo una actividad hidrotermal que produjo la alteración de los materiales con: (1) la génesis de nuevos minerales (esmectitas saponíticas y minerales del grupo de la serpentina) en los clastos de la roca caja incorporados a la brecha freatomagmática y (2) la recristalizacion de dolomita y sílice amorfa en las rocas carbonatadas más porosas desde el contacto hasta una distancia de aproximadamente 20 m. Sin embargo, las margas y los carbonatos micríticos no muestran recristalización, únicamente un ligero enriquecimiento en Mg y algunos elementos traza en los primeros metros cerca del contacto con la brecha freatomagmática y la lamproita.

Palabras clave: complejo freatomagmático-efusivo, alteración hidrotermal, saponita, provincia volcánica del SE español

1. Introduction

The term lamproite, which includes lamproites and kimberlites in the category of ultrapotassic rocks, was initially used by Niggli (1923) to identify high K and Mg rocks, and its use is recommended by the IUGS (Mitchell and Bergman, 1991). Lamproite magmas came from partially melted mantle at depths from 80 to 170 km (e.g. Prelević *et al.*, 2012),

although the depth proposed for the origin of the Spanish lamproite melts is considered slightly shallower, around 55-70 km (Contini *et al.*, 1993; Ferriz *et al.*, 1994; Solovova *et al.*, 1994). They are characterised chemically by high MgO and K_2O content and enrichment in incompatible elements. Typical minerals found in lamproite rocks include forsterite, leucite, phlogopite, and iron-rich sanidine.

The Volcano of Cancarix is an exceptional example of volcanic deposits characterised by phreatomagmatic activity followed by lamproitic extrusion (Seghedi *et al.*, 2007). One variety of lamproite, rich in enstatite, sanidine and phlogopite, is referred to as Cancalite or Cancarixite due to its occurrence at the Volcano of Cancarix (Parga-Pondal, 1935; Fúster *et al.*, 1967), though this term is not generally accepted.

The Volcano of Cancarix exemplifies part of a group of volcanic episodes that took place in southeastern Iberia during the Late Miocene (from 9.3 to 6.9 Ma, Duggen *et al.*, 2005; Pérez-Valera *et al.*, 2013), sometimes involving volcano edifices and/or dykes. The volcanoes of the lamproitic province of Albacete-Murcia-Almería —with main examples in Cancarix, Vera, Fortuna, and Jumilla— were initially studied in 1889 and have since become an international reference of lamproitic rocks (Fúster and Gastesi, 1965; Fúster *et al.*, 1967; Pellicer, 1973; Hall, 1987; Venturelli *et al.*, 1988; Mitchell and Bergman, 1991; Contini *et al.*, 1993; Linthout and Lustenhouwer, 1993; Salvioli-Mariani and Venturelli, 1996; Seghedi *et al.*, 2007; Prelević and Foley, 2007; Prelević *et al.*, 2008; Reolid *et al.*, 2009, 2013; Fritschle *et al.*, 2013). In the southern Iberian Peninsula, lamproitic bodies are associated with faults (Pérez-Valera *et al.*, 2010) and Neogene basins (Elizaga-Muñoz, 1994; Kuiper *et al.*, 2006). Spanish lamproites can be divided in two groups according to their content in SiO_2 and MgO (Duggen *et al.*, 2005). The group known as phlogopite lamproites shows relatively low SiO_2 and high MgO contents; it is developed on the Iberian crust and the Mesozoic sedimentary cover of Prebetic and Subbetic affinity. The other group, called lamproite derivates because they present higher SiO_2 and lower MgO contents than the typical lamproites, have been found only on the onshore Alborán domain. The Volcano of Cancarix is representative for the phlogopite lamproites and largest in size and preservation.

This article describes in detail the volcanic lamproitic edifice and its relationships with the sedimentary host rocks, whose interaction produced spectacular phreatomagmatic deposits and hydrothermal alteration in the host rocks. Such interactions have been poorly studied in the lamproitic outcrops of southern Spain to date (e.g. Seghedi *et al.*, 2007), in contrast with the geochemical and petrological aspects of lamproite (e.g. Fúster and Gastesi, 1965; López-Ruiz and Rodríguez-Badiola, 1980; Venturelli *et al.*, 1988; Linthout and Lustenhouwer, 1993; Salvioli-Mariani and Venturelli, 1996). The analysis of the phreatomagmatic deposits enabled us to reconstruct the genesis and evolution of the eruption. In this work we present additional informations and interpretations based on the detailed analysis of five sections from the phreatomagmatic deposits as well as textural, mineralogical and geochemical analyses of the different components of these phreatomagmatic deposits. In addition, changes in the host rock related to hydrothermal activity are also analysed.

2. Methods

Several field campaigns were carried out in the area, resulting in the elaboration of a detailed geological map (1:25000). This meant exploring and evaluating the different sides of the volcanic edifice very precisely. Five cross-sections were selected for sampling, to characterise the contact between the volcanic materials and the sedimentary host rocks. Altogether, forty-two samples —of both types— were collected. The cross-sections represent five margins of the volcanic edifice (West Quarry, Cancarix southwest, Cancarix northeast, Cancarix East and East Quarry).

Mineral composition was determined by X-ray diffractometry (XRD) using Cu-Kα radiation at 40 kV and 30 mA, in a Siemens D-5000 diffractometer (Universidad de Jaén). Unoriented powders were prepared using a holder filled from the side with halite as the internal standard. Oriented aggregates were prepared by sedimentation on glass slides. Ethylene glycol (EG) and dimethyl sulfoxide (DMSO) treatments were carried out on the aggregates to corroborate the identification of smectites and kaolinite.

Following XRD results and the optical microscopy study, ten samples were prepared as carbon-coated polished thin sections for Scanning Electron Microscopy (SEM) using back-scattered electron (BSE) imaging and energy-dispersive X-ray (EDX) analysis to obtain textural and chemical information. These observations were performed using a Zeiss DSM 950 SEM (Centro de Instrumentación Científica of the Universidad de Granada) equipped with an X-ray Link Analytical QX-20 energy-dispersive system (EDX). An accelerating voltage of 20 kV, with a beam current of 1-2 nA and counting time of 100 s, was used to analyse the silicates by SEM. The following compounds were used as calibration standards: albite (Na), periclase (Mg), wollastonite (Si and Ca), orthoclase (K), and synthetic Al_2O_3 (Al), Fe_2O_3 (Fe) and $MnTiO_3$ (Ti and Mn).

The transmission and analytical electron microscopy (TEM-AEM) studies were performed with two different microscopes: a Philips CM20 scanning transmission electron microscope (STEM) operating at 200 kV and with a LaB_6 filament (Centro de Instrumentación Científica of the Universidad de Granada) and a Jeol JEM 2100 STEM operating at 200 kV and with a point-to-point resolution of 2.5 Å in the TEM mode (Universidad Complutense of Madrid). Powdered portions were prepared using C-coated formvar Cu grids, and Cu rings were attached to representative selected areas of the thin-sections. Chemical analyses were made in the STEM mode with an EDX microanalyses system. Albite, biotite, spessartine, muscovite, olivine, titanite, MnS and CaS

were used as standards to derive K-factors for the transformation of intensity ratios to concentration ratios following the procedures of Cliff and Lorimer (1975).

Whole-rock analyses of five samples were carried out in the X-Ray Assai Laboratories of Lancaster (Ontario, Canada): a lamproite, the matrix of a phreatomagmatic breccia, and three marl-limestone rhythmites located at different distances from the breccia contact. X-ray fluorescence (XRF) was used for the major elements and inductively coupled plasma-mass spectrometer (ICP-MS) for the trace elements.

3. Geological setting and materials

The Volcano of Cancarix is located in the Sierra de las Cabras, South of Albacete province (southeast Iberian Peninsula, Fig. 1A), and just 2 km West of the village of Cancarix. All this area is included in the External Prebetic (Fig. 1B), the northernmost domain of the External Zones of the Betic Cordillera. The rocks constituting the main features of the Sierra de las Cabras are Jurassic carbonates corresponding to three formations (Figs. 1C and 2): (1) Massive

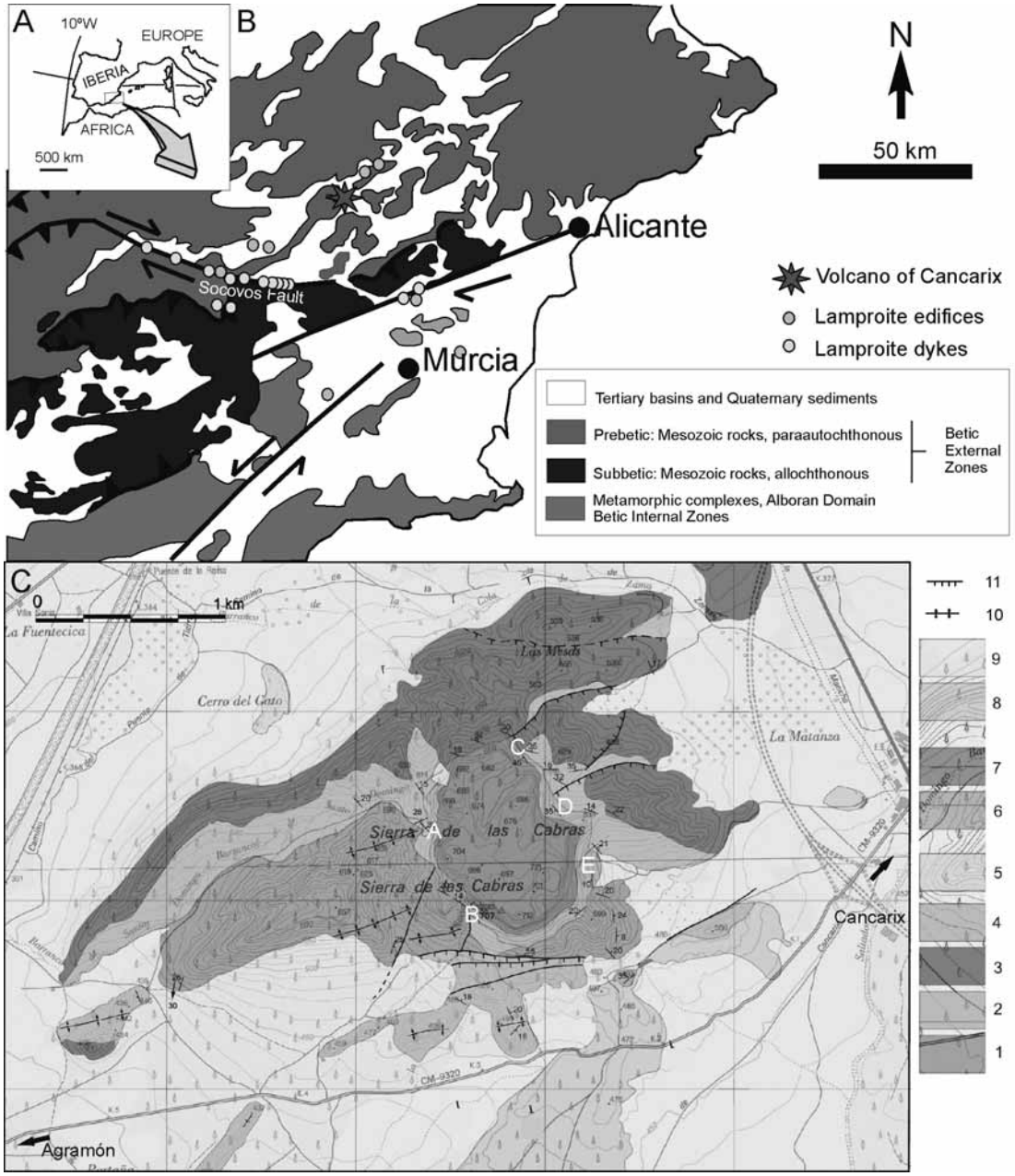

Fig. 1.- Location of the Volcano of Cancarix. A. Geographic location in Southern Spain. B. Geological map of the eastern end of the Betic Cordillera. C. Detailed geological map of the Sierra de las Cabras and the Volcano of Cancarix outcrop. Legend: 1. Massive limestones and dolostones (Middle Jurassic), 2. Marl-limestone rhythmite (Oxfordian-Lower Kimmeridgian), 3. Oncolitic limestones (Middle Kimmeridgian), 4. White limestones and marls (Cretaceous), 5. Calcarenites (Upper Miocene), 6. Phreatomagmatic complex (phreatomagmatic breccia, contact breccia, and lava; Upper Miocene), 7. Lamproite (Upper Miocene), 8. Conglomerates (Plio-Pleistocene), 9. Scree deposits (Pleistocene), 10. Antiform fold, 11. Normal fault. Letters A-E indicate studied sections distributed on the margins of the volcanic edifice: A, West Quarry; B, Cancarix southwest; C, Cancarix northeast; D, Cancarix East; E, East Quarry.

limestones and dolostones of the Middle Jurassic, with 60 m of well-bedded thick layers (>1 m). When dolomitisation is absent, the limestone textures are wackestones and oolitic grainstones; numerous banks show parallel lamination and the karstification is more intense. (2) Marl-limestone rhythmites of the Oxfordian-Lower Kimmeridgian, characterised by a 140 m thick alternance of marl and limestone beds (wackestone-packstones of peloids and quartz) disposed in an upward-thickening sequence. (3) Oncolitic limestones of the Middle Kimmeridgian, which comprise a well-stratified upward-thickening sequence (50 m thick), with a maximum bed thickness around 2 m. The oncolitic limestones are characterised by grainstones of oncoids (19 mm in diameter) with small colonies of corals. These are coarse grained limestones.

The Sierra de las Cabras is formed by a broad open anticline of axis approximately N080ºE, and features characteristics of a local anticlinorium (Fig. 1C). The folding affects the Mesozoic sedimentary sequence reaching the upper Miocene. South and East from the volcano the folds are cut by high-angle normal faults, N70–90ºE, dipping to the South. East of the volcano, the normal faults constitute a set of discrete planes that descend by the North limb, each single fault having a limited slip of a few tens of metres. West of the volcano, two faults with a cartographic strike slip of ~100 m limit the western sector of the anticlinorium, which remains free of faulting (Fig. 1C). This feature suggests that these strike-slip faults acted as lateral ramps or transfer of the aforementioned normal fault system. By contrast, normal faults South of the volcanic edifice coalesce in a broad fault damage zone that omits the Jurassic and sinks the Cretaceous sequence. This southern fault system limits Plio-Pleistocene conglomerate outcrops but cannot be followed by the scree Quaternary sediments that cover the area. The minimum throw of this fault zone, considering the Upper Jurassic sediment thickness (see below), is around 200 m. The age of the main faulting stage is Miocene and it is related with the Socovos Fault activity and the lamproites emplacement (Pérez-Valera *et al.*, 2013).

The main volcanic edifice is a cylindrical hill, 900 m in diameter and 250 m high above the surrounding valleys, that crops out in the axial zone of the anticlinorium (Figs. 1C and 3A). The most evident volcanic rocks constitute a body of massive lavas with a characteristic columnar jointing that is evident along a perimetral cliff, up to 100 m height (Fig. 3A and B). Vertical joints are pervasive, with a predominant metric spacing, but a quarry escarpment shows that joints are curved at the base (Fig. 3B). In the eastern wedge of the volcanic edifice, the columnar jointing is superimposed on a banded structure resembling horizontal stratification (Fig. 3C). In the inner parts of the volcanic edifice, spheroidal weathering creates rounded boulders of lamproite (40 cm to 4 m in diameter) (Fig. 3D). The main massive lamproite edifice is almost completely surrounded by a phreatomagmatic tuff ring of variable thickness (Reolid *et al.*, 2013), usually

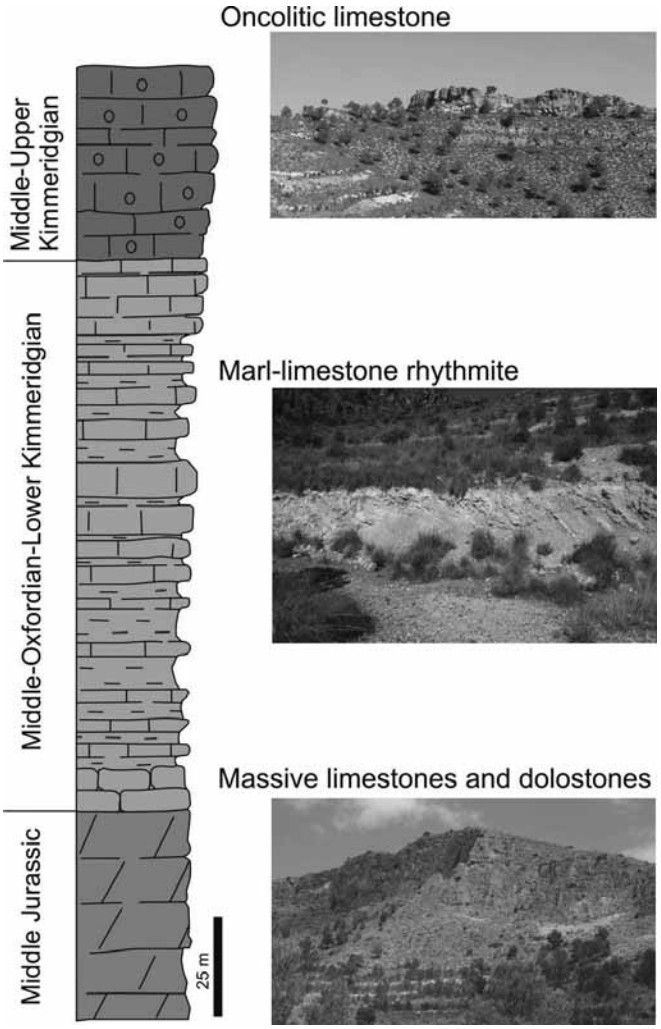

Fig. 2.- Jurassic stratigraphy of the Sierra de las Cabras and images of the different formations constituting the host rocks of the Volcano of Cancarix.

< 22 m, yet greater when the host rock is the mechanically less competent marl-limestone rhythmite (Fig. 1C). The phreatomagmatic ring consistently dips 20–30º towards the centre of the volcanic edifice. The higher values of dipping are at the southwest edge. The tuff ring is better developed South and East of the edifice; elsewhere the thickness decreases, particularly to the North and southwest, where the main lava body is almost in direct contact with the Jurassic carbonates (Fig. 1C). Contact of the lamproitic body with the pyroclastic beds of the phreatomagmatic-effusive complex is planar to irregular, depending on the autobrecciation of the lava at the boundary.

A smaller outcrop of volcanic rocks is separated from the main edifice. It is situated in the continuation of the southern normal fault system (Fig. 1C). It has a maximum length of 100 m and is made of lava flow and volcanic ash. Quaternary sediments shelter the relationship between these lavas and the host rock. This body can be interpreted as a lateral conduit of the main volcanic edifice (Reolid *et al.*, 2013).

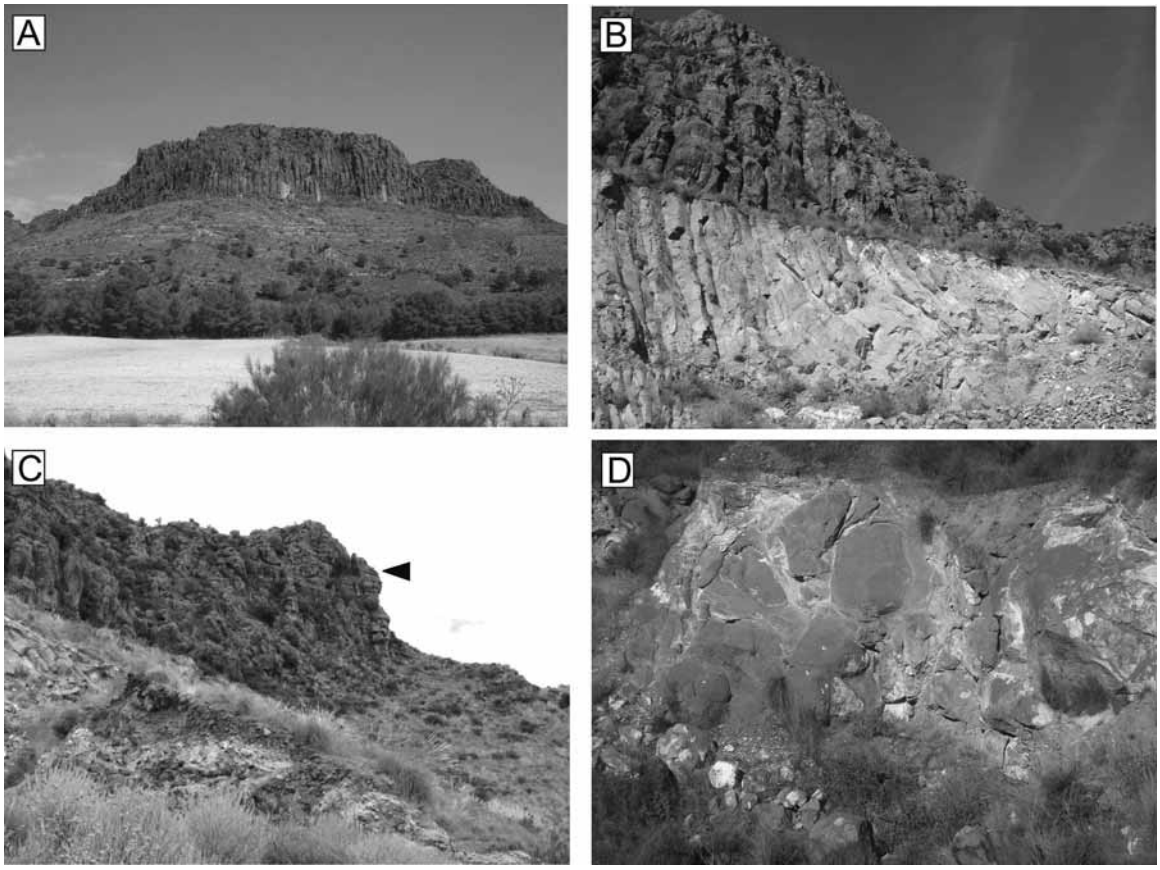

Fig. 3.- Aspect of the Volcano of Cancarix and jointing. A. Landscape view of the South face of the outcrop and the columnar jointing. B. Curvature of the columnar jointing closest to the contact with the phreatomagmatic-effusive complex in the East Quarry. C. Columnar jointing superimposed on a banded structure resembling horizontal stratification (arrow) from the East wedge (in the first plane, phreatomagmatic-effusive complex). D. Rounded boulders of lamproite from the inner parts of the volcanic edifice created by spheroidal weathering.

4. Phreatomagmatic-effusive complex

The studied sections distributed on five margins of the volcanic edifice (West Quarry, Cancarix southwest, Cancarix northeast, Cancarix East and East Quarry; Fig. 1C) present a thickness of the phreatomagmatic-effusive complex ranging from 8 to 24 m. Three different lithologies can be differentiated in the phreatomagmatic-effusive complex (phreatomagmatic complex in Reolid *et al.*, 2013). According to a general stratigraphic order they are:

a.- Contact breccia, consisting only of carbonate clasts derived from the immediately surrounding host rocks (mainly massive limestones) (Fig. 4). The clast size is usually from 1 to 30 cm, but exceptionally ranges from 7 m maximum diameter down to microscopic size. The clasts are mostly angular to subangular, and locally exhibit jigsaw-fit textures (Lorenz and Kurszlaukis, 2007). The smallest clasts constitute the cemented carbonate matrix. The contact breccia is associated with the West edge of the main volcanic edifice.

b.- Phreatomagmatic breccia organised in beds, generally without grading, having a metric-scale thickness and high lateral variability (Fig. 5). The breccia is composed by a grey-to-white matrix (<2 mm in size) constituted by small grains of host sedimentary rocks and volcanic rocks (from lava fragments and lapilli-size pyroclasts to coarse ash) (Fig. 6A and E). The proportions of pyroclasts and fragments of sedimentary rocks are variable. The breccia is darker when volcanic material predominates. White carbonate clasts (5–100 cm) are calcinated fragments of sedimentary rocks (Figs. 5D and 6) and present spectacular white to pink alteration rings (Figs. 6B and 6C). The blocks composed by large fragments broken from previously consolidated lava (Fig. 5) are usually angular and show different textures, from fluidal with phenocrysts of forsteritic olivine, to highly vesicular scoriaceous. Subspherical vesicular clast up to 45 cm in diameter are resembling ballistical bombs. Some large pyroclasts with fluidal texture include white carbonate clasts (Fig. 6D).

c.- Lava interlayers of metric-scale beds (<3 m) pinch out laterally a few metres (Figs. 5 and 7). Two main types of lava may be differentiated: a) massive lava (sometimes clastogenic, produced by autobrecciation) with bedding (Fig. 7A); and b) banded vesicular lavas having a fluidal laminated texture and different vesicular density, with forsterite phenocrysts (Figs. 7B-F).

Figure 8 shows the distribution of the three components of the phreatomagmatic-effusive complex along the five studied

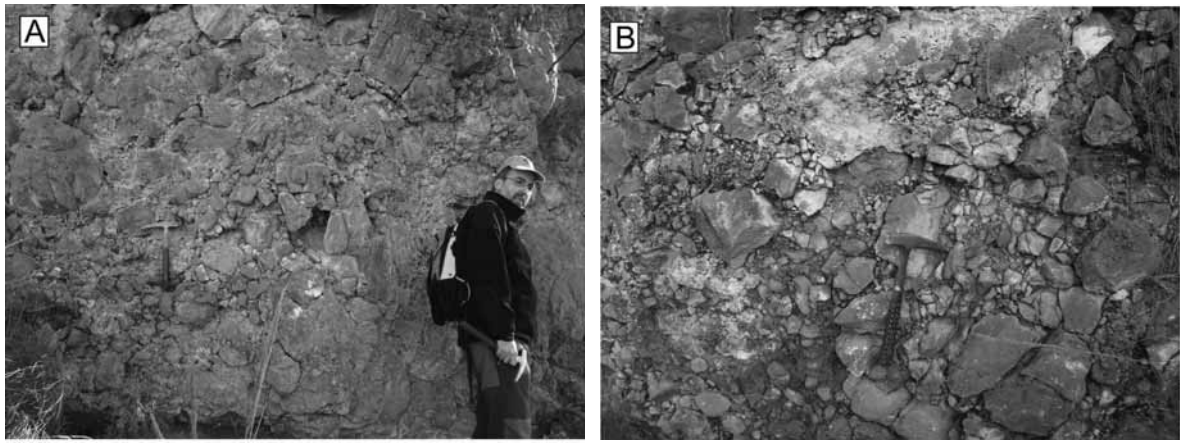

Fig. 4.- Contact breccia at the base of the West Quarry section. The clasts are composed of dolostones and massive limestones of the Middle Jurassic and a minority from the oncolitic limestone of the Middle Kimmeridgian.

sections. The contact breccia is very well exposed only in the West Quarry section, with a maximum thickness of 17.1 m that progressively decreases toward the eastern parts of the phreatomagmatic ring. In the same sense, the thickness of the phreatomagmatic breccia and the lava interlayers increases. Following a stratigraphic sequence from the carbonate host rock at the base to the lamproite edifice, the contact breccia, if present, is at the lower part of the sections. After the contact breccia, the phreatomagmatic breccia with lava interlayers is recorded. The white carbonate clasts are dominant at the base of the phreatomagmatic breccia and decrease progressively upwards; meanwhile, pyroclasts and lava interlayers increase upwards. As a general trend, the diameter of pyroclasts increases upwards. The fluidal vesicular lava interlayers are

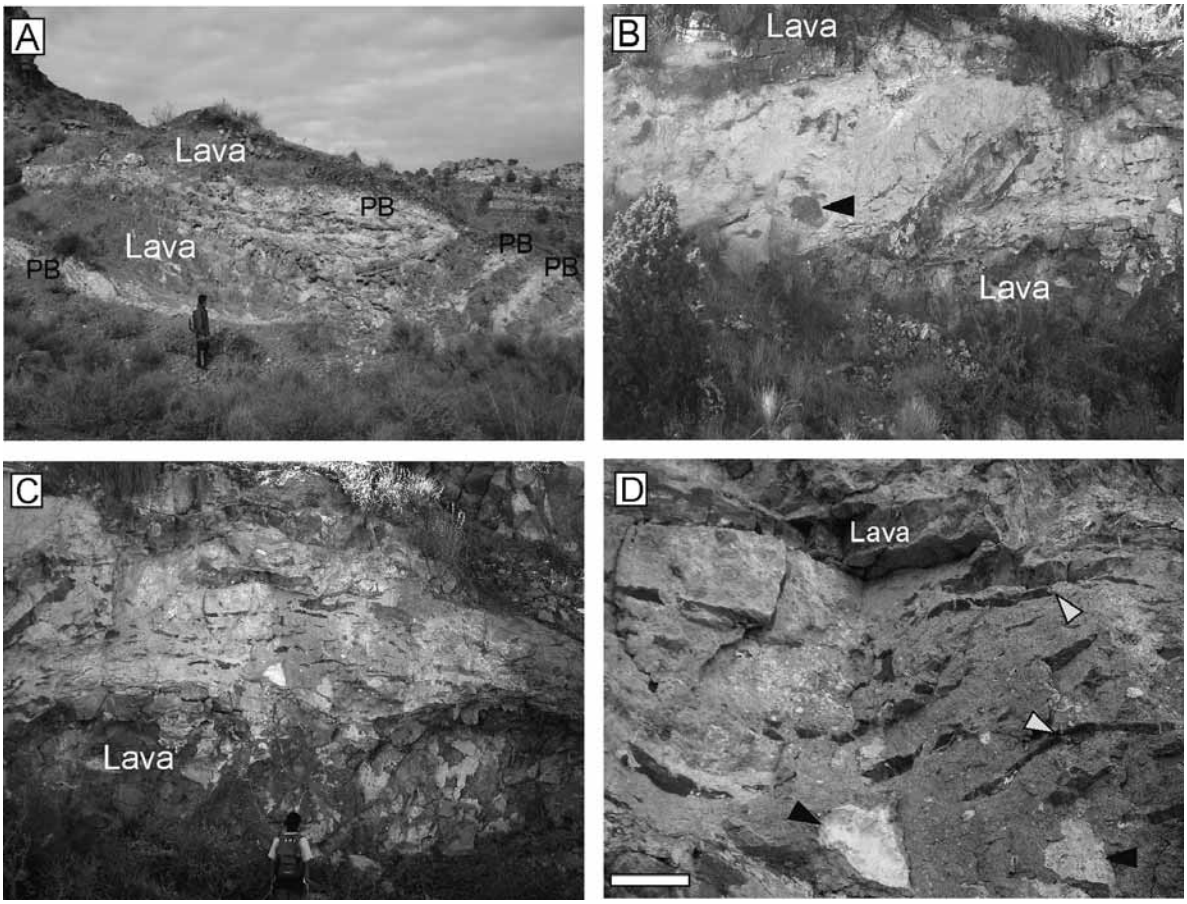

Fig. 5.- Different aspects of the phreatomagmatic breccia in the East Quarry. A. Geometric relations between the phreatomagmatic breccia (PB) -light colour- and the lava intervals with different thickness and dark colour. B. Lava beds, stratiform lava fragments (like flaser structures) and pyroclastic bombs (arrow) within the phreatomagmatic breccia. C. Interval with phreatomagmatic breccia showing common fragments of lava beds and white clasts. D. Detail of the previous image with indications of the lava flasers (yellow arrows) and large white clasts (black arrows). Scale bar = 30 cm.

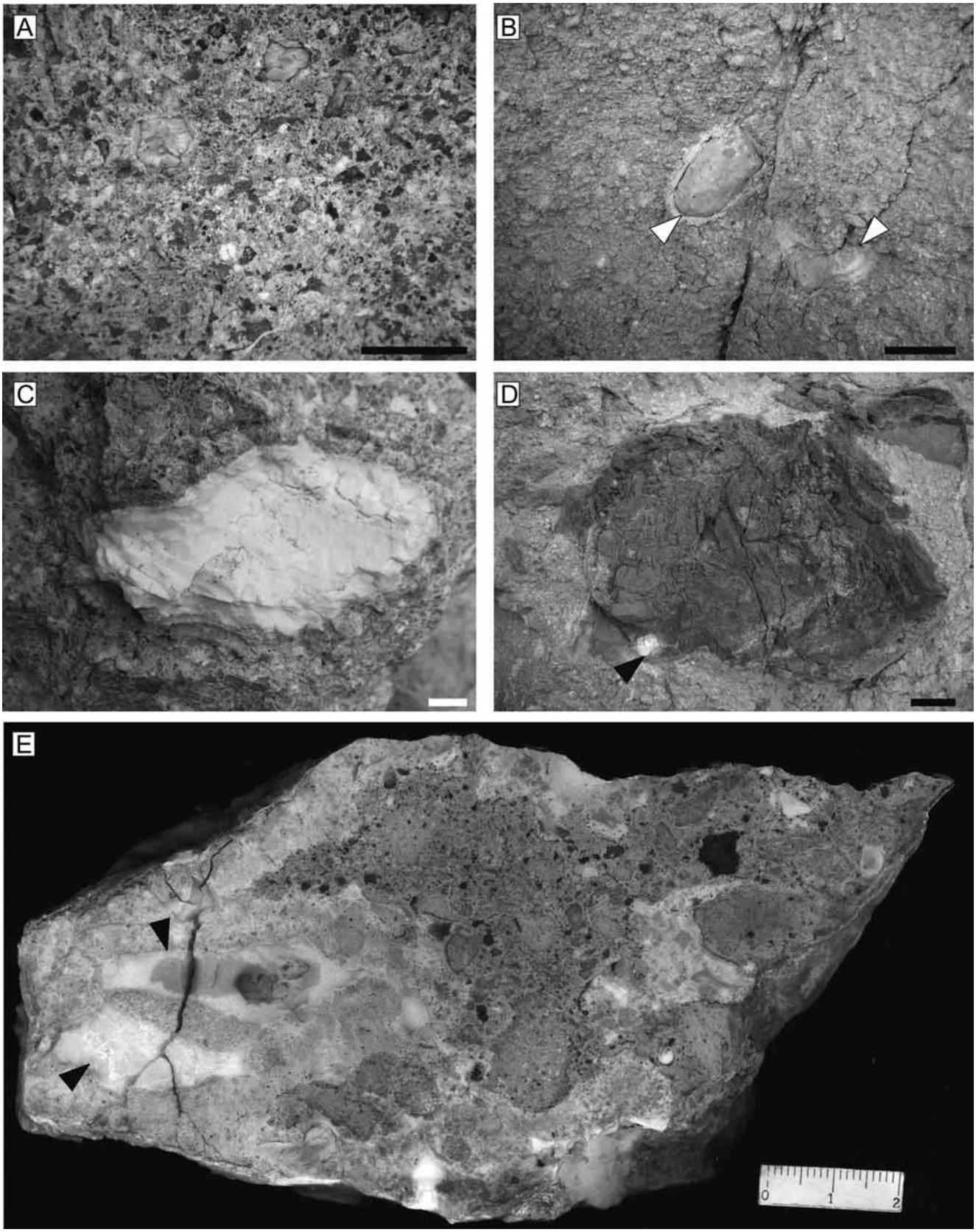

Fig. 6.- Details of the phreatomagmatic breccia in the East Quarry. A. Matrix of the phreatomagmatic breccia with carbonate grains (white) from the host rocks, vesicular lapilli (grey grains) and enstatite crystals (green grains). Scale bar = 1 cm. B. White clasts (arrows) with alteration haloes in a matrix of lapilli and ashes. Scale bar = 5 cm. C. Fragment of host rock preserved as a white clast with a concentric pink alteration halo. Scale bar = 1cm. D. Pyroclastic bomb with fluidal and vesicular texture and a white clast included (arrow). Scale bar = 10 cm. E. Polished slab of phreatomagmatic breccia with carbonate-dominated matrix including white clasts (arrows) and dark parts with pyroclastic-dominated volcanic matrix.

dominant with respect to the clastogenic massive lava interlayers, which are more common at the upper part of the East Quarry section.

5. Mineralogical and geochemical characterisation

This section is focused on the mineralogical, geochemical and textural features of the phreatomagmatic deposits and the altered host rocks (marl-limestone rhythmite and oncolitic limestones) surrounding the lamproitic edifice as a consequence of the volcanic activity. Previously, there is a brief description of the lamproites.

5.1. Lamproites

The studied volcanic outcrops are constituted by lamproites composed by forsteritic olivine, Ti phlogopite, diopside, enstatite, richterite with Ti and K, leucite, and Fe-rich

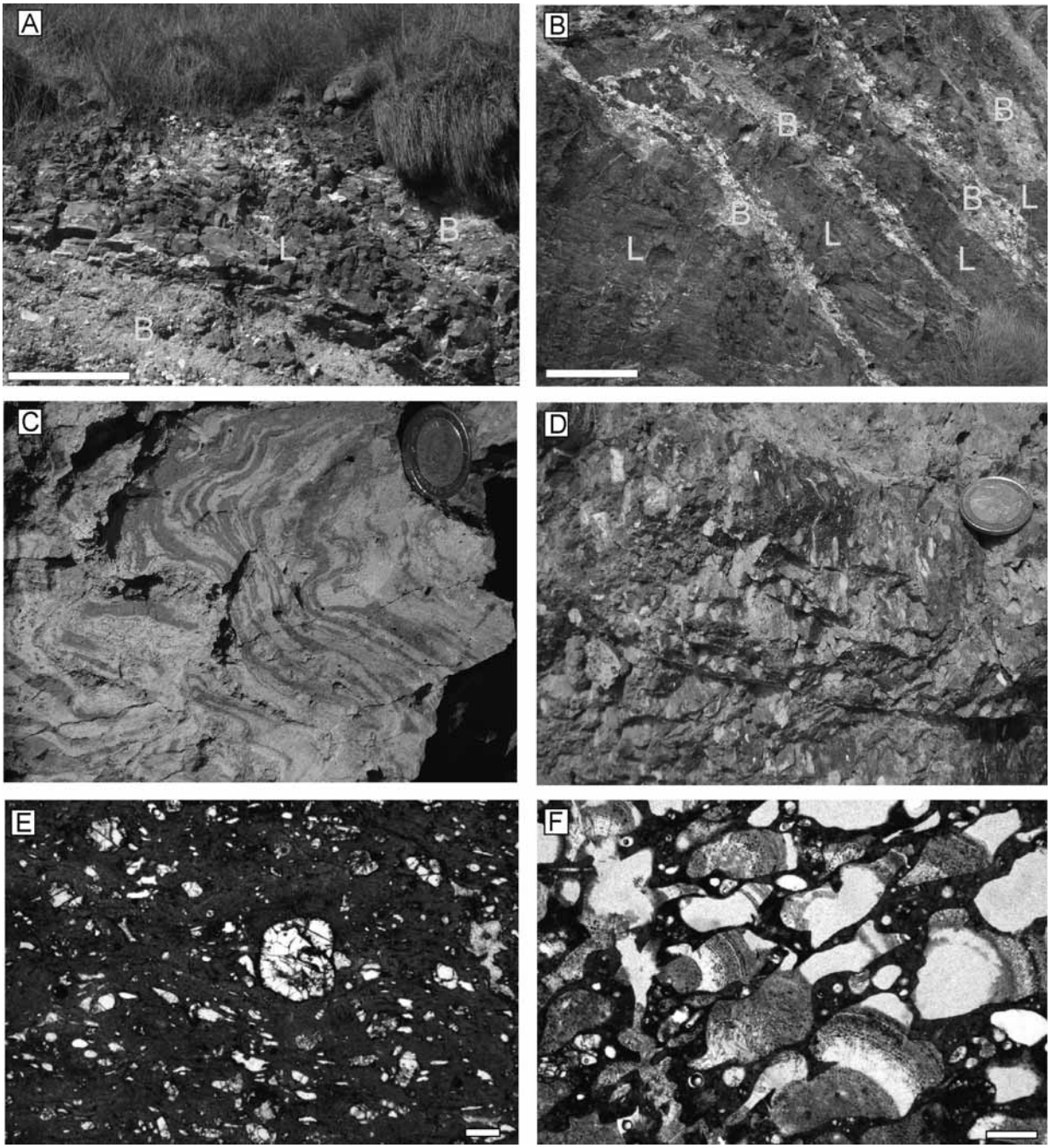

Fig. 7.- Field, hand and microscopic views of the lava deposits in the phreatomagmatic-effusive complex. A. Alternance of phreatomagmatic breccia (B) with massive clastogenic lava (L) from the East Quarry (scale bar = 1 m). B. Alternance of banded vesicular lavas (L) and phreatomagmatic breccia (B) from the East Quarry (scale bar = 1 m). C. Fluidal laminated texture from Cancarix southwest section. D. Highly vesicular lava from the West Quarry. E. Lava with forsterite phenocrysts from the Cancarix southwest section (scale bar = 1 mm). F. Highly vesicular lava with scarce olivine phenocrysts and vesicles infilled by sanidine from the West Quarry section (scale bar = 1 mm).

sanidine. According to Fúster *et al.* (1967), the mineralogical and textural features depend on the crystallisation degree. Olivine almost disappears in the holocrystalline inner parts of the lamproitic main body, but is locally common in the glassy lavas where there is a porphyric texture with glassy to microcrystalline groundmass. Phlogopite and diopside are mainly present in holocrystalline rocks as subhedral and euhedral crystals (Fig. 9), while amphibole and sanidine appear as interstitials sometimes developing poikilitic crystals. The geochemistry of these rocks is extremely unusual due to the high contents in MgO, K_2O, P_2O_5, Ni, Cr, Rb, Ba, Th, and Zr (Table 1).

5.2. Matrix of the phreatomagmatic breccia

The phreatomagmatic breccia XRD patterns show the presence of clay minerals (smectites and serpentine minerals) in addition to enstatite, quartz and carbonates (calcite and dolomite) (Fig. 10A). The XRD diffractogram corresponding to the matrix of the phreatomagmatic breccia (Fig. 10B) shows a clear enrichment in clay minerals and a minor presence of carbonates. Green crystals with xenomorphic and hypidiomorphic habit (Fig. 6A) were observed and analysed by SEM; they correspond to enstatite $(Si_{1.89}\ Al_{0.20})O_4(Al_{0.19}\ Fe_{0.11}\ Mg_{1.48}\ Ti_{0.01})\ Ca_{0.15}$. Enstatite crystals are surrounded by calcite crystals (Fig. 11A) and a very fine-grained matrix composed mainly by clays (Fig. 11B). Figure 11C shows phenocrysts of forsterite $(Fe_{0.16}\ Mg_{1.82})\ SiO_4$. The smectites of the matrix are mainly trioctahedral smectites (Mg-rich saponite-like composition, Table 2). At the lattice scale, smectites show a texture with slightly curved and discontinued packets of 10 Å layers (Fig. 11D).

5.3. Lava interlayers from phreatomagmatic-effussive complex

The lava interlayers present almost exclusively forsterite phenocrysts under petrographic microscope (Figs. 7E, F). However, the XRD analysis of one of these lava layers, par-

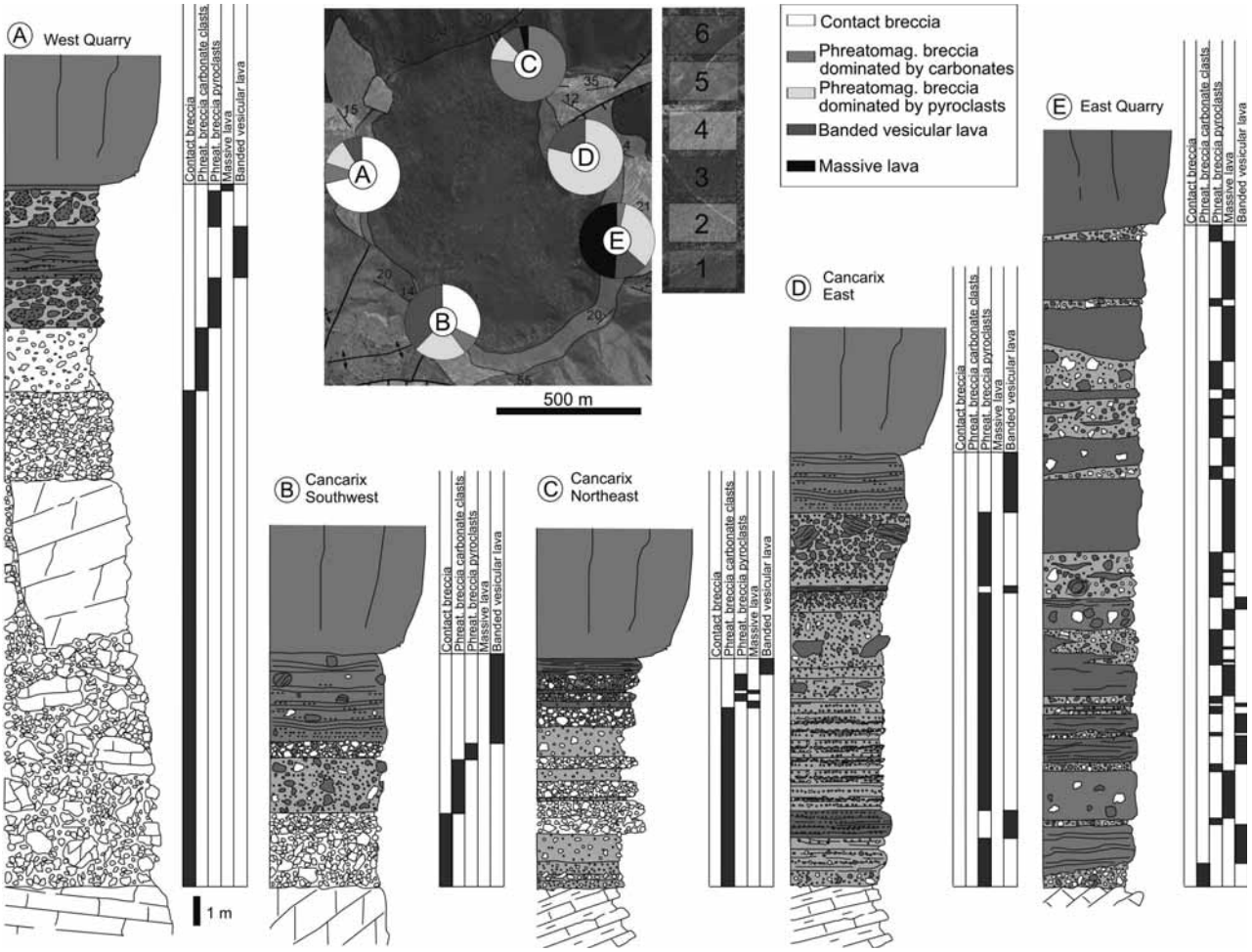

Fig. 8.- Studied phreatomagmatic sections with distribution of the contact breccia, phreatomagmatic breccia rich in carbonate clasts, phreatomagmatic breccia rich in pyroclasts, massive lava and banded vesicular lava. The host rocks are the lower boundary and the lamproites with columnar jointing are the upper boundary. The geological map represents the location of the sections and the proportions of the components of the phreatomagmatic-effusive complex (pie diagrams). Legend for geological map: 1. Massive limestones and dolostones (Middle Jurassic), 2. Marl-limestone rhythmite (Oxfordian-Lower Kimmeridgian), 3. Oncolitic limestones (Middle Kimmeridgian), 4. White limestones and marls (Cretaceous), 5. Phreatomagmatic-effusive complex (Upper Miocene), 6. Lamproite (Upper Miocene).

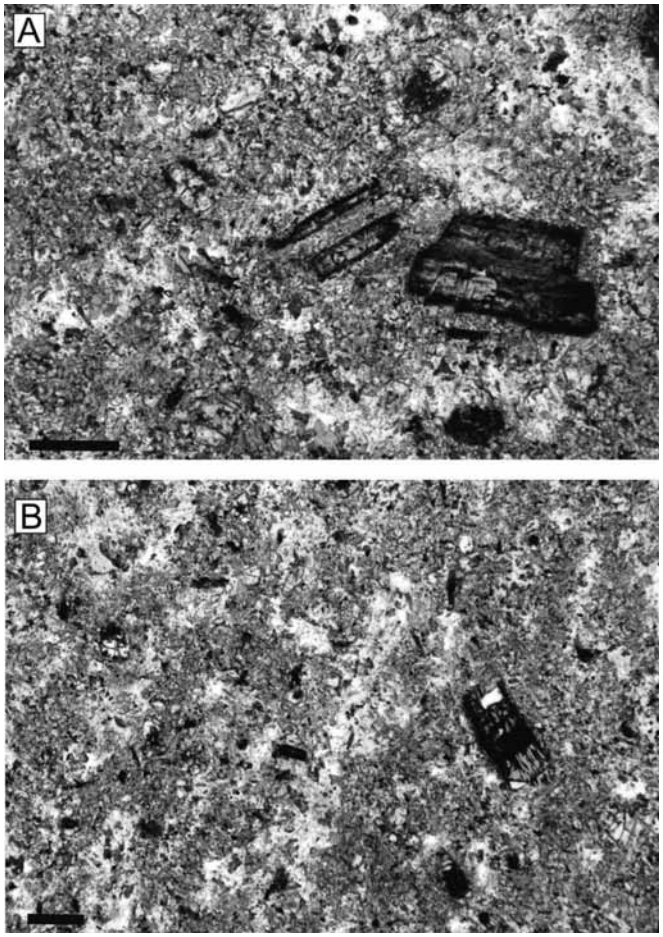

Fig. 9.- Holocrystalline texture of the lamproite with phlogopite and amphibol embedded in a microcrystalline matrix of sanidine from inner parts of the lamproite dome. Scale bar = 1 mm.

tially altered and intercalated in the phreatomagmatic breccia, presents a mineral association of phlogopite, sanidine, leucite, amphibols, augitic piroxenes, smectite and vermiculite (Fig. 10C). TEM-AEM microanalyses of smectites reveal an Mg-rich trioctahedral saponite-like composition. The chemical composition of amphibols is very rich in K, with values around 1.5–2 atoms per formula unit (a.f.u.).

5.4. Host rocks

The emplacement of the volcanic edifice affected the marl-limestone rhythmite and oncolitic limestones, promoting in situ mineralogical changes as well as the genesis of white carbonate clasts incorporated into the phreatomagmatic breccia and xenoliths in the lamproites.

Marl-limestone rhythmite

The marl-limestone rhythmite was sampled along the same bed at different distances from the volcanic edifice in order to check potential effects on the mineralogy and geochemistry related to the volcanic emplacement in the host rock. In the outcrop, the most evident effect on the marls and lime-

	Lamproite	Phreat. breccia	Marls (0.9 m)	Marls (8 m)	Marls (40 m)
SiO_2	38.56	24.48	16.66	32.13	12.58
Al_2O_3	5.85	7.39	5.19	7.17	4.28
Fe_2O_3	3.44	2.42	1.76	2.13	1.41
MnO	0.051	0.028	0.02	0.031	0.016
MgO	14.97	21.25	14.94	10.75	2.43
CaO	12.1	33.49	23.89	17.76	41.46
Na_2O	0.51	0.3	0.07	0.16	0.07
K_2O	2.4	1.17	1.47	2.05	0.86
TiO_2	0.951	0.348	0.251	0.393	0.168
P_2O_5	0.58	0.16	0.12	0.07	0.04
L.O.I.	-	8.52	27.18	27	26.23
Sc	8	6	4	6	4
Be	11	3	2	2	1
V	51	55	41	55	31
Cr	400	50	30	30	30
Co	22	3	2	5	< 1
Ni	390	80	70	< 20	20
Cu	20	30	10	< 10	20
Zn	70	30	40	30	< 30
Ga	12	12	9	9	6
Ge	1.2	0.9	0.9	0.7	< 0.5
As	65	5	5	< 5	< 5
Rb	150	94	87	100	51
Sr	486	184	131	121	390
Y	17.3	22	15.5	20.9	10.6
Zr	501	110	80	118	44
Nb	24.1	7.4	5.1	7.4	3.8
Sn	8	3	2	3	1
Sb	5.9	0.5	3.7	7.3	0.5
Cs	27.3	12.1	18.5	15.5	4.6
Ba	537	265	189	218	108
La	61.5	26.3	17.9	23.3	12.4
Ce	164	43.8	30.1	44.7	18.7
Pr	23.3	5.17	3.46	5.46	2.25
Nd	88.1	19	12.8	18.2	8.11
Sm	19.5	4.06	2.75	3.8	1.77
Eu	3.18	0.803	0.559	0.76	0.364
Gd	10.1	3.39	2.39	3.52	1.52
Tb	0.91	0.56	0.37	0.57	0.25
Dy	3.65	3.08	2.1	3.07	1.47
Ho	0.57	0.61	0.41	0.57	0.29
Er	1.48	1.79	1.22	1.64	0.84
Tm	0.209	0.26	0.182	0.242	0.12
Yb	1.22	1.56	1.15	1.57	0.71
Lu	0.173	0.227	0.16	0.238	0.101
Hf	14.7	2.8	2	3.1	1.1
Ta	2.03	0.79	0.53	0.8	0.34
W	3.2	5.3	3.8	3.6	1
Tl	0.85	0.43	0.67	0.79	0.26
Pb	31	6	7	7	7
Th	65.2	7.66	5.11	6.93	3.48
U	12.2	3.96	2.69	2.54	2.18

L.O.I.: Loss of ignition.

Table 1.- Chemical composition (wt % and ppm) of the studied materials, lamproites, matrix of the phreatomagmatic breccia and marls at different distances to the contact (0.9 m, 8 m and 40 m).

stones closer to the phreatomagmatic-effusive complex is the intense red colour (Fig. 12). Yet three metres away from the contact, the marl-limestone rhythmite has the characteristic yellow to white colour.

The XRD patterns of the marls closest to the phreatomagmatic breccia show a dominant carbonate composition, mainly dolomite and secondarily calcite. Other components are quartz and phyllosilicates, mainly mica (muscovite and biotite). BSE images (Fig. 13) show crystals of dolomite, silicates with detrital appearance (K-feldspars with rutile inclusions, quartz, tri- and dioctahedral micas, chamositic chlorites and zircons) and very fine-grained kaolinite (Table 3).

The distance to the volcanic rocks does not imply significant mineralogical differences in the closest 25 m of the marl-limestone rhythmite. In samples farther from the volcanic edifice, however, calcite is the dominant carbonate instead of dolomite. Regarding the silicates, quartz and a very minor proportion of micas are present.

The geochemical composition of the marl, according to a proximal-distal transect with respect to the lamproite edifice, is consistent with the mineralogy recorded (Table 1). The Mg content is higher in the analysed marly bed closer to the phreatomagmatic breccia, given the abundance of dolomite and the influence of the lamproite edifice as a source of Mg. The Mg content tends to decrease from the lamproite-phreatomagmatic breccia to the reddish marls-yellow marls (see Table 1). This trend is paralleled by other elements, such as Ni, Rb, Cs, Ba, U, Th, Be, Cr, Zr and Co.

Oncolitic limestones

The oncolitic limestones show textural and mineralogical changes, which vary according to the proximal-distal gradient to the volcanic edifice. In a distance >20 m the oncolitic limestones do not show evidence of alteration, but relatively closer samples present a progressive increase in small rhombohedral crystals in the original sparitic cement of the oncolitic grainstone (Fig. 14A). These new crystals, white in hand sample, are yellow cream to dark brown in thin section and grow preserving the ooids and peloids located in the sparitic cement. Their altered aspect is characterised by darker edges. EDX-SEM microanalyses of the rhombohedral crystals indicate a solid solution between calcite and dolomite with a proportion of Mg always lower than Ca. The darker parts of these crystals are enriched in Si. The opacity of the grains increases with the content of Si and suggests the record of

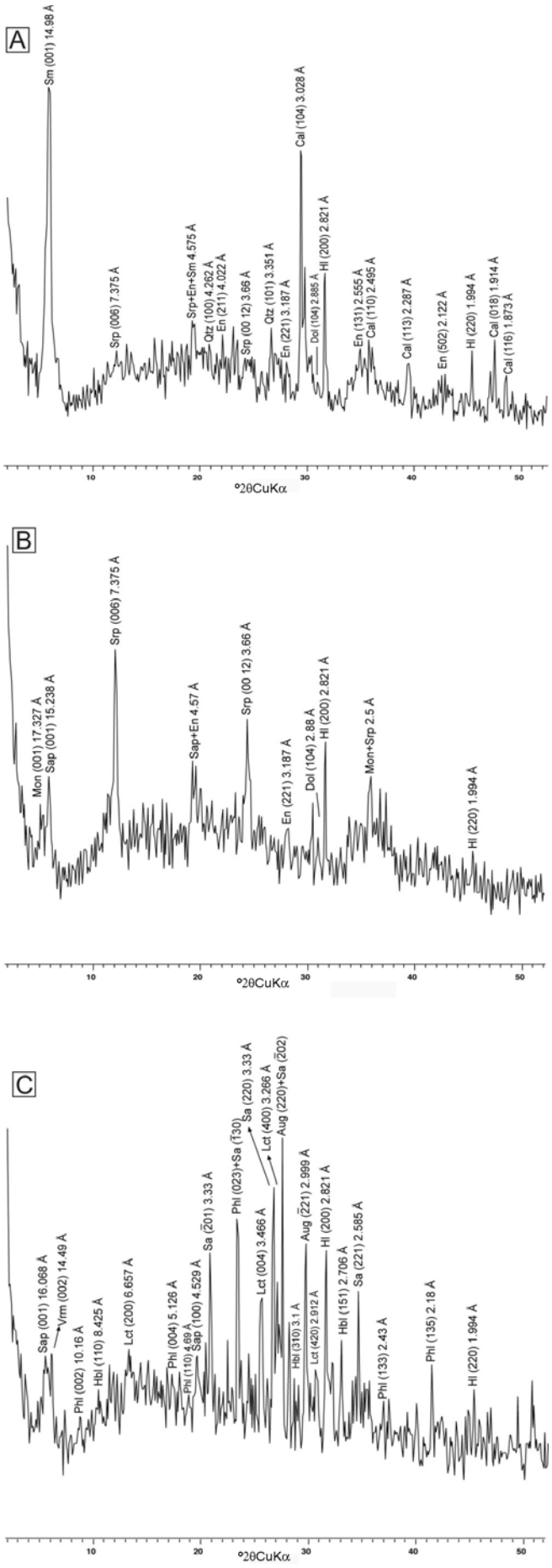

Fig. 10.- X-ray diffraction patterns of the phreatomagmatic breccia from the East Quarry. A. Sample of the phreatomagmatic breccia. B. Sample exclusively of the matrix of the phreatomagmatic breccia. C. Sample from the altered lava included in the phreatomagmatic breccia. Note that the abbreviations used are those proposed by Kretz (1983): Aug = augite, Cal = calcite, Dol = dolomite, En = enstatite, Hbl = hornblende, Lct = leucite, Mon = montmorillonite, Phl = phlogopite, Qtz = quartz, Sa = sanidine, Sap = saponite, Sm = smectite, Srp = serpentine group minerals, Vrm = vermiculite, and Hl = halite (internal pattern).

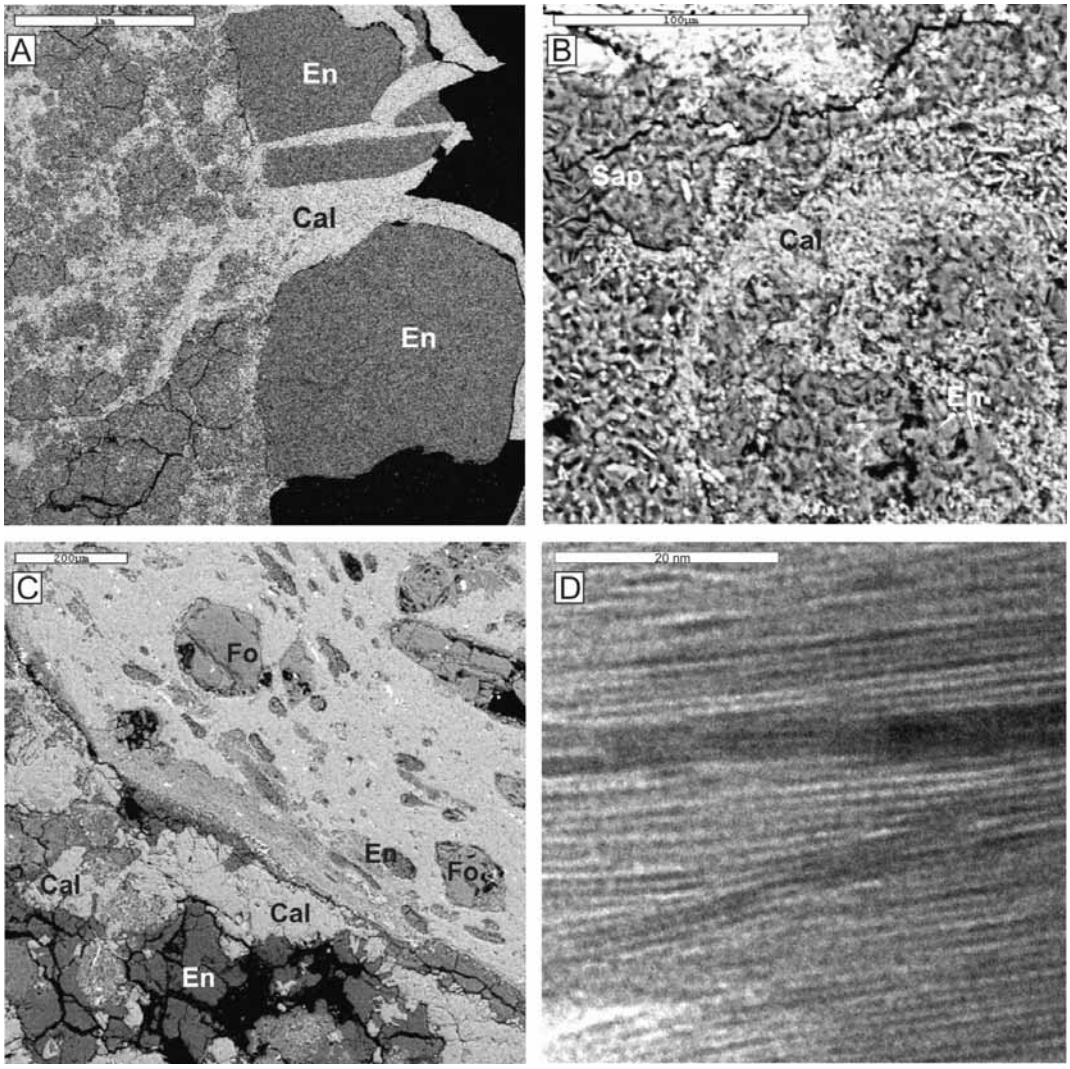

Fig. 11.- Electron microscopy images from the phreatomagmatic breccia from the East Quarry. A and B. BSE images of the phreatomagmatic breccia, which is composed by calcite (Cal) and enstatite (En) immersed in a matrix mainly composed by clays (saponite, Sap). C. BSE image including a fragment of lava with forsteritic olivine (Fo) and enstatite (En). D. Lattice-fringe image showing an area with thin packets in which 10 Å periodicity predominates (dehydrated smectite).

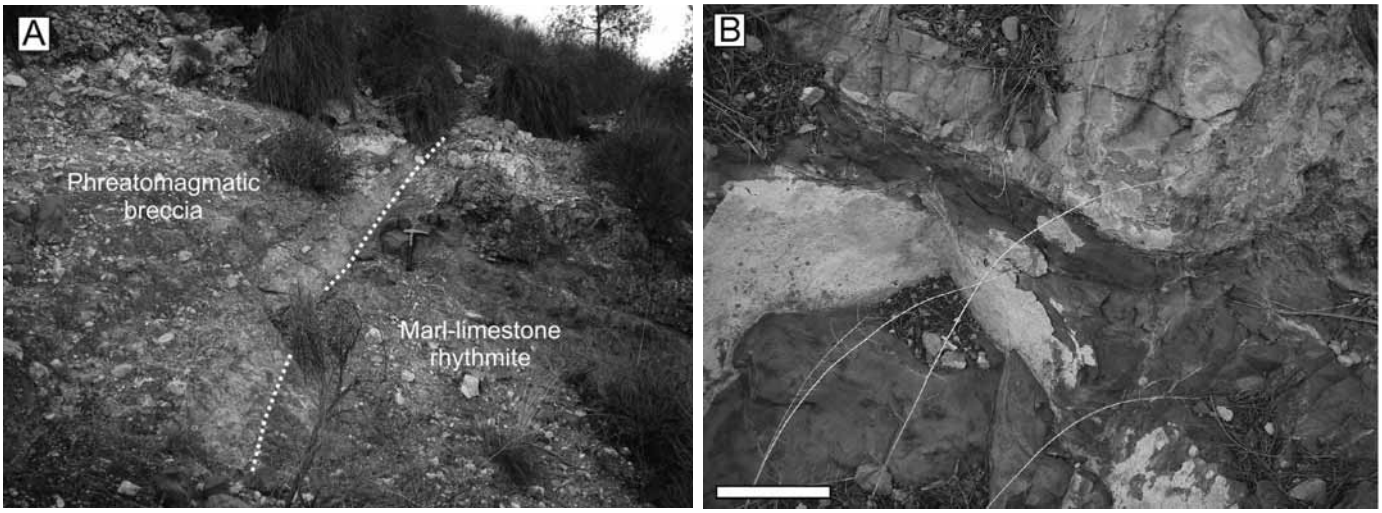

Fig. 12.- Contact between marl-limestone rhythmite and the phreatomagmatic breccia from the Cancarix northeast section. Scale bar = 10 cm.

	Si	^{IV}Al	^{VI}Al	Fe	Mg	Ti	∑oct.	K	Na	Ca	∑ inter.
CX-6b_2 4	3.38	0.62	0.00	0.42	2.54	0.04	3.00	0.14	0.01	0.20	0.35
CX-6b_2 5	3.18	0.81	0.00	0.50	2.67	0.00	3.17	0.01	0.00	0.25	0.27
CX-6b_2 6	3.14	0.86	0.11	0.33	2.69	0.01	3.15	0.01	0.02	0.20	0.23
CX-6b_2 7	3.16	0.84	0.12	0.34	2.54	0.03	3.03	0.01	0.02	0.28	0.31

EDX-SEM microanalyses

Table 2.- Structural formula for smectites of the sedimentary material normalized to $O_{10}(OH)_2$.

		Si	^{IV}Al	^{VI}Al	Fe	Mg	Ti	∑oct.	K	Na	Ca	∑ inter.
CX-8b_1 1	1	3.12	0.88	1.80	0.06	0.21	0.00	2.07	0.89	0.04	0.01	0.94
CX-8b_6 3	2	3.05	0.95	1.82	0.06	0.11	0.06	2.05	0.83	0.08	0.01	0.92
CX-8b_6 4	3	3.05	0.95	1.83	0.04	0.13	0.02	2.03	0.85	0.09	0.01	0.98
CX-8b_1 3	4	2.62	1.38	0.66	1.07	0.98	0.15	2.85	0.61	0.03	0.04	0.68
CX-8b_1 4	5	2.70	1.30	0.62	1.09	0.97	0.12	2.79	0.74	0.06	0.03	0.83
CX-8b_1 7	6	3.07	0.93	0.47	0.98	1.19	0.10	2.74	0.67	0.05	0.04	0.76
CX-8b_6 7	7	3.95	0.05	3.84	0.01	0.14	0.00	4.00	0.17	0.00	0.04	0.20

1-3: muscovites, 4-6: biotites normalized to $O_{10}(OH)_2$; 7: kaolinite normalized to $O_{10}(OH)_8$.

		Si	^{IV}Al	^{VI}Al	Fe	Mg	Mn	Ti	∑oct.
CX-8b_3 1	1	2.75	1.25	1.19	2.71	2.10	0.02	0.00	6.03
CX-8b_4 3	2	2.86	1.14	1.29	2.73	1.85	0.04	0.01	5.92

chlorites normalized to $O_{10}(OH)_8$.
EDX-SEM microanalyses

Table 3.- Structural formula for phyllosilicates in the marl-limestone rhythmite.

amorphous silica. Locally, very fine-grained Mg smectites were identified.

At a distance of 5 m from the lamproite contact the new crystals form a continuous mass among the oncoids (Fig. 14B). The smaller grains —ooids, peloids and bioclasts— are consumed by the growth of the rhombohedra, now larger and darker due to the increase in amorphous silica content. The dissolution/crystallisation advances following the sparitic cement, while the oncoids are preserved as relicts resisting the growth of the rhombohedra due to low porosity and the presence of dense micritic laminae in concentric coats acting as a barrier. At any rate, isolated idiomorphic crystals grow inside the oncoids. The new crystals locally appear with dissolved margins.

At the lamproite-oncolitic limestone contact, all the sparitic cement and the oncoid edges were re-emplaced by a new generation of carbonate crystals (Fig. 14C). The inner parts of the oncoids show a recrystallisation by xenomorphic sparitic calcite, and only occasionally an oncoid preserving remains of the original oncolitic lamination is recorded (micritized oncoids).

White carbonate clasts of the phreatomagmatic deposits

These are calcareous clasts from the host rock located inside the phreatomagmatic breccia and locally in the lava beds (Figs. 5 and 6). These calcareous fragments present different altered features depending on the temperature conditions undergone and the nature of the original rock (massive limestones and dolostones of the Middle Jurassic, marl-limestone rhythmite of the Oxfordian-Lower Kimmeridgian or oncolitic limestones of the Middle Kimmeridgian). The porosity, water content, presence of phyllosilicates (especially in marls and marly limestones) and the size of the clasts are factors controlling the final texture. In any case, clasts with a very high content in carbonates are recrystallised, having lost the original sedimentary fabric. When the recrystallisation degree is low it is possible to identify traces of the sedimentary fabric, including microfossils. The size of the white clasts ranges from a few centimetres to exceptionally 1 m.

Many clasts from the marl-limestone rhythmite are characterised by low density and concentric bands. The most evident textural changes are alteration rings or haloes (Fig. 6B, C and 15 A, B). The microscopic analyses evidence a diffuse texture with calcite crystal balls (Fig. 15A). XRD patterns of marly limestones clasts show a composition of mainly calcite and clay minerals such as trioctahedral smectites and lizardite, a mineral of the serpentine group (Fig. 15C). SEM reveals that the crystals of calcite present Si and a Ca content lower than 1 a.f.u. (0.7–0.8 a.f.u.). It is possible to infer contamination by amorphous silica and to consider the presence of CaO in the external haloes located in the margins of the white carbonate clasts as a product of calcination. Other white clasts with concentric haloes show the same mineralogy, but the calcite crystals are not observable (Fig. 15B). White clasts coming from the oncolitic limestones of the Middle Kimmeridgian evidence the same features as at the contact between the lamproites and the oncolitic limestones on the North side of the volcanic edifice (Fig. 14C).

Xenoliths

Two main types of xenoliths, located in the West side of the volcanic edifice, can be recognised in the lamproites, ac-

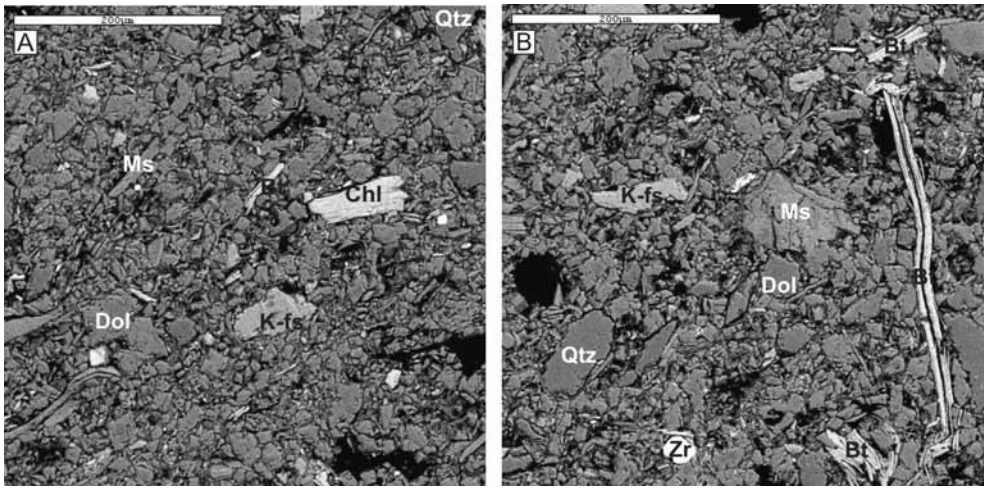

Fig. 13.- BSE images of the marl-limestone rhythmite mainly composed of dolomite (Dol) and detrital minerals in the Cancarix northeast margin. Bt = biotite, Chl = chlorite, K-fs = K-feldspar, Ms = muscovite, Qtz = quartz, Zr = zircon.

cording to the original composition of the host rock: massive limestones and dolostones of the Middle Jurassic (Fig. 16A, B) and marly limestones of the Lower Kimmeridgian (Fig. 16C, D). In both cases these sedimentary-derived xenoliths, ranging from 3 cm to 1m, form discrete patches of rather clear rock within the lamproite. Their clear outlines suggest that they have not been assimilated by the magma.

The xenoliths composed originally by massive limestones or dolostones have a strongly recrystallised and brecciated appearance, featuring jigsaw-fit textures (Fig. 16A). From the compositional point of view they present enrichment in amorphous silica. The marly limestones xenoliths, some of them included in vesicular lava layers just below the lamproitic edifice, are composed of carbonates, amphibols, quartz, K-feldspar and clay minerals (smectite and serpentine minerals).

6. Interpretation

6.1. Origin and evolution of the volcano

The Volcano of Cancarix is a small edifice that implies a relatively limited emission of magma, which required the aid of a free pathway along the crust, such as a fault or fault zone. There is no chief structure with a clear expression on the surface as occurs in nearby lamproitic outcrops (Pérez-Valera *et al.*, 2013), though a volcanic-diapiric alignment has been proposed (Jerez-Mir, 1973; Rodríguez Estrella, 1979). The extrusion of the magma appears to be associated with the normal and strike-slip local fault systems that shaped the Sierra de las Cabras (Reolid *et al.*, 2009; Pérez-Valera *et al.*, 2013), probably during the Late Miocene.

The folding is previous to the faulting stage, thus most likely unrelated with the magmatism extrusion. On the other hand, although the volcanic outcrops are not faulted, there is a close relationship between outcrop distribution and shape, and fault distribution (Fig. 1C), suggesting that the volcanic eruptions took place during or immediately after the faulting. In this sense, the $^{40}Ar/^{39}Ar$ age of the volcanic rocks at 7.0 Ma (Duggen *et al.*, 2005) is congruent with the supposed age of faulting during the Upper Miocene. Moreover, lamproitic dykes, with a similar composition intruded along the neighbouring Socovos Fault, where they have been interpreted contemporaneous with the fault movement (Pérez-Valera *et al.*, 2010, 2013). Therefore, fault activity could be related with magma ascent in depth determining the final point of emplacement at the surface.

The effusion of the igneous rocks took place in two clearly different phases: a) an initial highly explosive phase, dominated by phreatomagmatic eruption as a result of the interaction between the magma and the phreatic water contained in the karstic system and in the fractures of the host Jurassic calcareous rocks; and b) a second phase dominated by the emission of lava, producing the filling of the crater where the lamproitic materials are more crystalline. Consequently, massive lava were deposited over the phreatomagmatic-effusive complex (Fig. 17).

According to this phreatomagmatic eruptive model, the initial explosions increased the diameter of the central vent of the volcano, producing a progressively wider crater (Fig. 18). The subsequent explosions led to underground fragmentation of the host rock, resulting in contact or explosive breccias (Grady and Kipp, 1987; Lorenz *et al.*, 2002; Lorenz and Kurszlaukis, 2007). The phreatomagmatic-effusive complex shows alternance between lava flows and phreatomagmatic breccia beds, which suggests an open system in the magma/phreatic water interaction. Lava flows correspond to effusive episodes between phreatomagmatic explosive activities. Aranda-Gómez and Luhr (1996) and Risso *et al.* (2008) propose this type of open system with different phases and a variable water input for examples from Mexico and Argentina. The intervals dominated by massive lava (sometimes clastogenic, produced by autobrecciation) in the phreatomagmatic-effusive complex are located atop the phreatomagmat-

ic sections and suggest a decrease in the interaction processes between magma and phreatic water, as indicated by Seghedi *et al.* (2007). The intervals dominated by phreatomagmatic breccia indicate new water inputs producing phreatomagmatic explosions and the incorporation of abundant sedimentary rock fragments resulting later in white carbonate clasts.

The moderate vesicularity of pyroclasts, mainly lapilli size, indicates that vesicular texture in the magma developed early during the phreatomagmatic fragmentation by magma-phreatic water interaction (Németh *et al.*, 2007). The high content of white carbonate clasts in the phreatomagmatic breccia suggests a transport of pyroclasts through a relatively narrow conduit in the first phases of eruption, when the conduit was unstable and collapse episodes of the explosion chamber were more likely.

The phreatic water inputs to magma were controlled by jointing sets of the host rocks and the karstic system. Massive limestones and dolostones were the rocks with the highest groundwater flow, due to the penetrating jointing sets and the karstic system developed in these fractures. These rocks allowed the input of groundwater to the phreatomagmatic system. Lorenz and Kurszlaukis (2007) and Kurszlaukis and Lorenz (2008) propose a general model of phreatomagmatic eruptions with some aspects compatible with the Volcano of Cancarix features. According to this model, phreatomagmatic thermohydraulic explosions initially happen close to the surface and become progressively deeper with the advance of explosive activity (Fig. 18). This process produces an increase in the depth and diameter of the crater. Successive explosions produce host rock fragmentation, resulting in

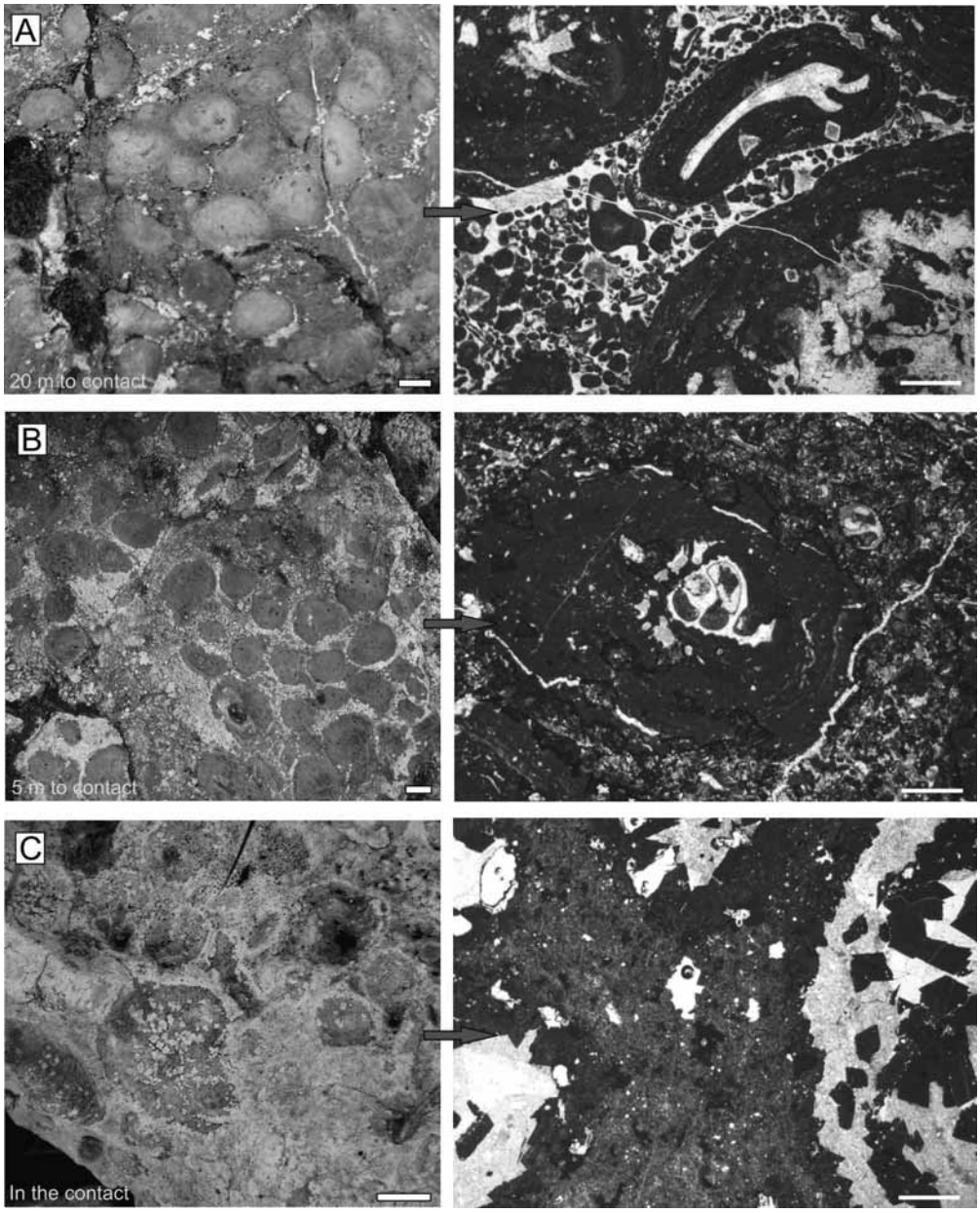

Fig. 14.- Field close view and microscopic view of the Kimmeridgian oncolitic limestones at different distances from the contact in the North margin. Scale bars for field views 1 cm and for microscopic views 1 mm. See explanation in the text.

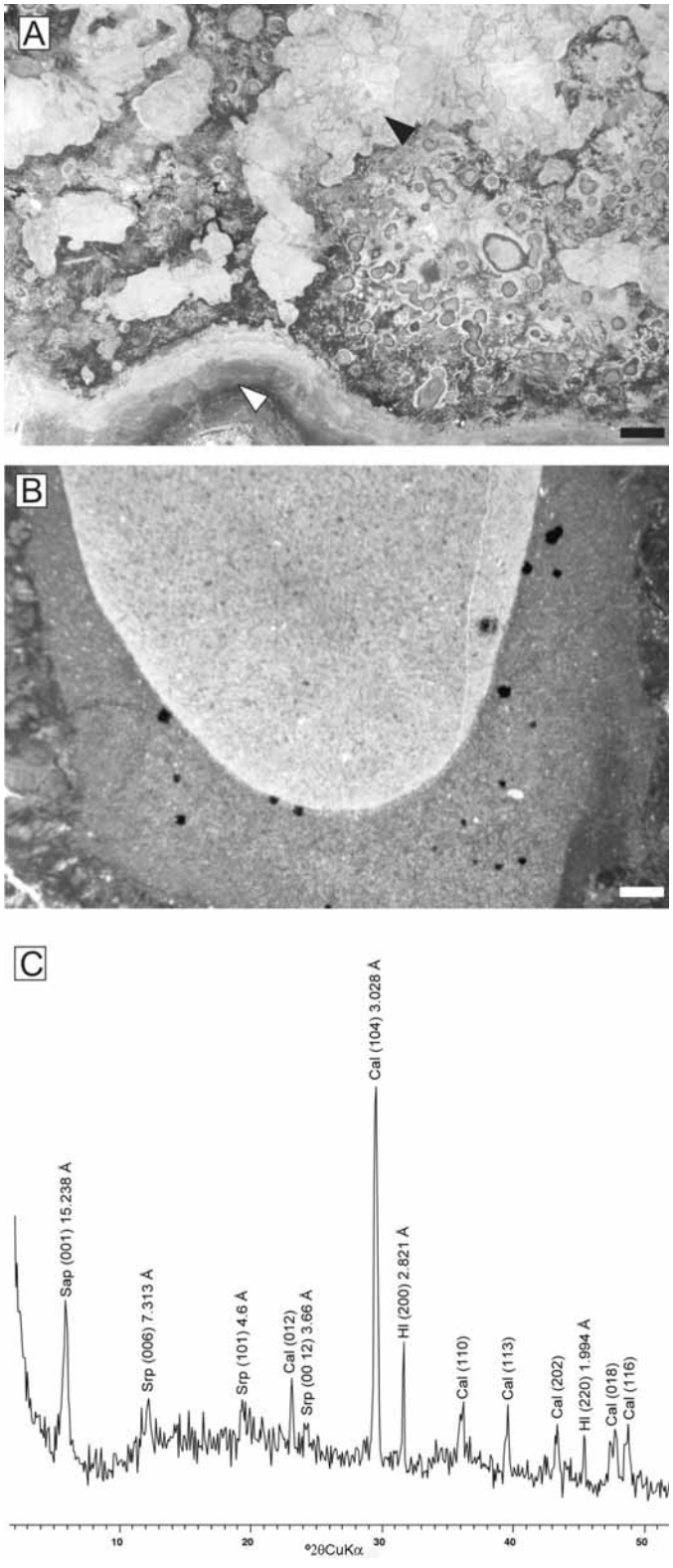

Fig. 15.- Two different aspects of the white carbonate clasts of the East Quarry under petrographic microscope and XRD pattern. A. Areas with calcite recrystallisation (black arrow) and calcite crystal balls. White arrow indicates the alteration halo (scale bar = 1mm). B. White clast of marly limestone with alteration halo (scale bar = 1mm). C. XRD analysis of white carbonate clasts. Note that the abbreviations used are those proposed by Kretz (1983): Cal = calcite, Sap = saponite, Srp = serpentine group minerals, and Hl = halite (internal pattern).

contact or explosive breccia (Grady and Kipp, 1987; Lorenz *et al.*, 2002; Lorenz and Kurszlaukis, 2007). The effective underground fragmentation of once normally jointed and unweathered massive limestones requires a mechanical process entailing a high stress rate. In other words, it would have required an explosion (Grady and Kipp, 1987; Lorenz and Kurszlaukis, 2007), during which the host rocks were affected first by a shock wave, then by a rarefaction wave (Fig. 18). These contact breccias may collapse downward (total or partially) on the chamber formed by the previous explosion. After each explosion, the explosion chamber (*s*. Lorenz and Kurszlaukis, 1997) is temporarily evacuated by the eruption, giving a cavity filled in by the wall collapse with volcanic rock fragments as well as carbonate host rock fragments (the future white carbonate clasts, Fig. 18B). New magma inputs reach the explosion chamber and press on contact breccia, which may have phreatic water arriving from the host rock fractures by means of the piezometric gradient. This process produces new evaporation of water close to the magma and the increase of pressure in the explosion chamber, favouring another phreatomagmatic explosion (Fig. 18C). Because the water vapour has high pressure and temperature during the thermohydraulic phreatomagmatic explosion, it rapidly drives the expansion of gas to the surface, moving out great amounts of clasts from the contact breccia (Lorenz *et al.*, 2002).

When the input of outside water from the host rock decreased, the eruption became drier and evolved, according to Seghedi *et al.* (2007) towards Strombolian fallout episodes with intercalated clastogenetic lava flows (Hawaiian-style). The water availability decreased as eruption continued, as a consequence of the exhausting of the outer water sources from the host rock and continuous magma supply. Subsequently, the highly viscose degasified crystalline magma advanced over the phreatomagmatic-effusive complex filling the crater. This second stage of the eruption is discussed by previous authors. According to Mitchell and Bergman (1991) this second phase resulted on a lava lake, nevertheless Seghedi *et al.* (2007) proposed an extrusive dome formed by viscose magma. From our observations, more crystallized magma suggests high viscosity and the curvature of the columnar jointing to the base on the East edge point to extrusive lava dome as documented in other European examples (Hetényi *et al.*, 2012).

The phreatomagmatic ring consistently dips 20–30º towards the centre of the vent and indicates the partial collapse of the crater walls after the phreatomagmatic explosive phase. This allows us to interpret the geometry of the walls during the Strombolian eruption phase. The dipping of the walls was lower toward the East edge of the volcano, at the contact with the marl-limestone rhythmite, and coincides with the thicker phreatomagmatic-effusive complex (Fig. 8).

The volcanic vent that fed the system is situated close to the West edge. This is deduced from: a) the tectonic structure of the Sierra de las Cabras, b) the highest values of dipping

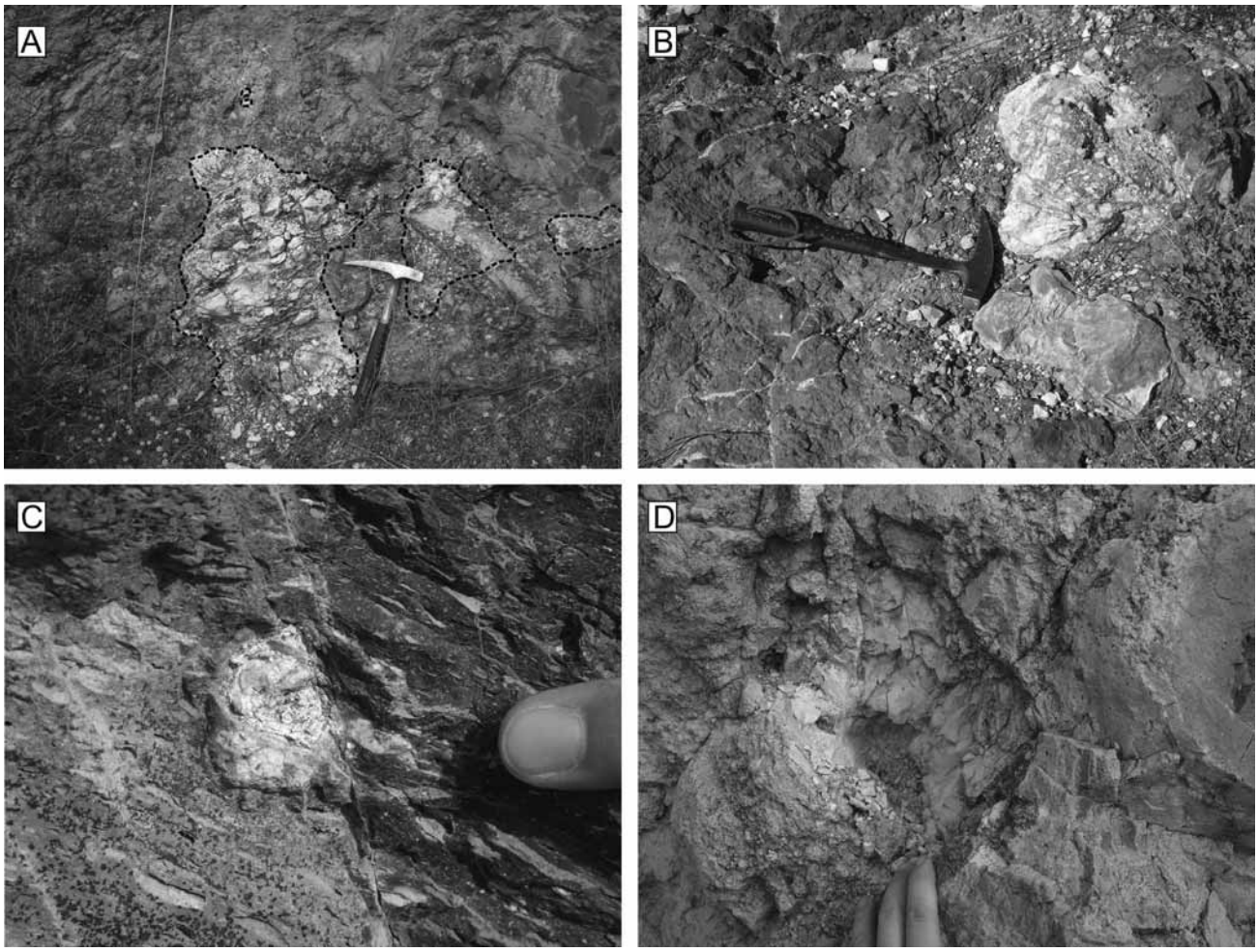

Fig. 16.- Xenoliths from the West face of the crystalline lamproitic edifice. A and B: Xenoliths from massive limestones and dolostones of the Middle Jurassic included in the crystalline lamproitic edifice close to the Cancarix southwest. C and D: Xenolith from marly limestones of the Lower Kimmeridgian included in vesicular lava layers just below the crystalline lamproitic edifice close to the West Quarry.

of the phreatomagmatic breccia at the southwest edge, c) the highest content of contact breccia on the West edge (Fig. 8), d) the record of host rock xenoliths West of the lamproite edifice (Fig. 16), e) the absence of phreatomagmatic-effusive complex in the northwest edge (Fig. 1C), f) the curvature of the columnar jointing to the base on the East edge, indicating the lateral palaeo-boundary of the lava flow, and the lesser thickness of the lamproitic edifice in this sector (Fig. 3B), and g) the banded structure resembling horizontal stratification observed in the East wedge, likewise indicating the lava flow (Fig. 3C). Lamproites cover the vent located close to the northwestern sector, whereas the lava flows advanced mainly to the southeast, favoured by the presence of host rocks with less strength. For instance, the marl-limestone rhythmite may create a depressed palaeo-topography compared with massive limestones and dolostones of the Middle Jurassic and oncolitic limestones of the Upper Jurassic (see the geological map of Fig. 1C). This palaeo-topography controlled the eruptive process and the thickness and dipping of the phreatomagmatic-effusive complex (thicker and having less dip over marl-limestone rhythmite).

6.2. Hydrothermal alteration processes

The first phase of the effusion of the igneous rocks —which promoted initial dehydration, cracking and hydrofracturing in the host materials— was very explosive and dominated by phreatomagmatic eruption. Afterwards, further explosions led to the advance of fragmentation, generating contact or explosive breccias. As a consequence of these processes, the surrounding carbonates and marls underwent mineralogical and textural changes. According to several authors (Dennis *et al.*, 1982; Bühmann, 1992; Bishop and Abbot, 1995), the size of the igneous body is one factor conditioning effects on sedimentary host rocks. Other important variables are the temperature of the melt, the fracture network and texture of the country rock, the fluids and the fluid fluxes. Central volcanoes, which are fixed in space, permit much longer intervals of high-temperature hydrothermal systems than those at mid-ocean ridges, with new crust continually moving out. Another factor to take into account is the depth of emplacement. When it is close to the terrestrial surface or on the surface, cooling is faster than when the emplacement

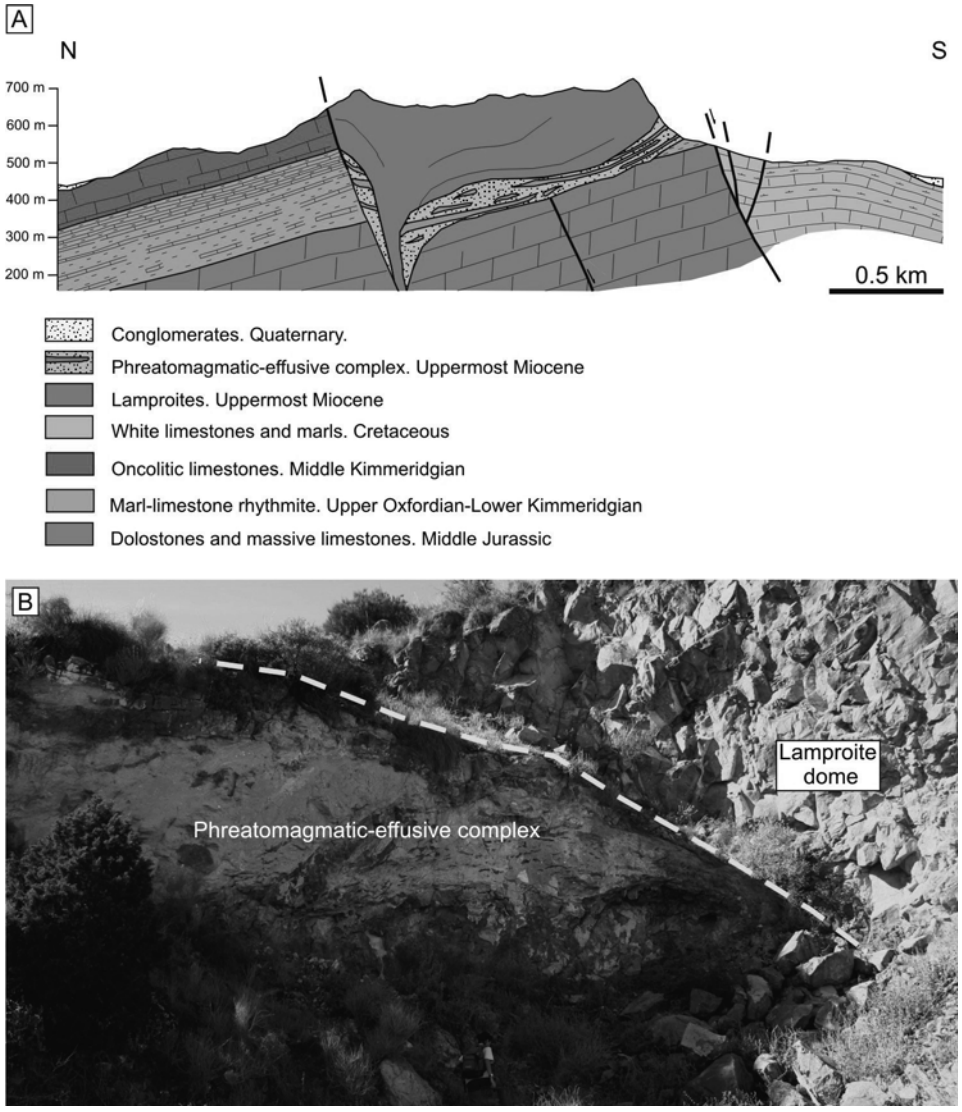

Fig. 17.- Disposition of the lamproites over the phreatomagmatic-effusive complex. A. Geological cross-section. B. Contact of the lamproite edifice with the phreatomagmatic complex in the East margin, close to the East Quarry.

is deep, resulting in short heating times and smaller intervals for changes. In the case of the Volcano of Cancarix, as previously mentioned, the extrusion of the magma appears to be related to the normal and strike-slip local fault systems that shape the Sierra de las Cabras, which suggests rapid cooling. In any case, the chemical, textural and mineralogical data of the host rocks clearly reveal a process of recrystallisation in the carbonates, above all in the metres closest to the contact with the igneous materials, due to the increasing temperature and the circulation of hydrothermal fluids in the surroundings of the volcanic activity.

The geochemical data along the transect lamproite - phreatomagmatic breccia - marls of the host rock (marl-limestone rhythmite) point to a decrease in the contents of the most characteristic components of lamproite (MgO, K_2O, P_2O_5, Ni, Cr, Rb, Ba, Th and Zr). The marls close to the phreatomagmatic breccia present higher values in these elements, which progressively decrease farther from the phreatomagmatic ring. The chemistry of lamproite is key to explain the high content of dolomite in the carbonate rocks surrounding the volcano, instead of calcite as it happens in the farthest host rocks. A good example of this feature is found in the oncolitic limestone, where the dolomite crystals are described as small euhedral grains (rombohedra) dispersed in the original sparitic cement, together with amorphous silica and Mg-smectites, 30 m from the volcano. Nevertheless, the proportion of these minerals increases according to the proximity to the lamproite; by the contact of the oncolitic limestone with the lamproite (North face, Fig. 1) the dolomite constitutes a continuous mass of crystals among the oncoids, which are recrystallised by xenomorphic calcite (Fig. 14). These textural and mineralogical data point to a hydrothermal alteration that favoured the development of dissolution-recrystallisation processes. These processes were more accentuated at the contact with the lamproitic body, where the temperature would have reached the highest values for the longest

duration, as deduced from its crystallinity compared to the lava layers of the phreatomagmatic-effusive complex. In subaerial hydrothermal systems like this, fluids can recirculate and boiling can occur, causing precipitation of hydrothermal minerals and even the partitioning of gases such as CO_2 in the vapour phase; it may condense later near the surface, producing carbonate-rich surface groundwaters. Whereas the recent emplacement of the lamproites affected the sparitic cement of the oncolitic limestone (due to the porosity and the coarse grained texture), which shows the advance of hydrothermal fluids among grains, the micritic coating of the oncoids would be more resistant to alteration (due to the scarce porosity and fine grained texture). Finally, by the contact with the lamproites the oncoids would have recrystallised during a later superimposed hydrothermal event under cooler conditions, after the total replacement of the sparitic cement by dolomite and amorphous silica. Silicification processes are common in the later stages of the hydrothermal cycle, when

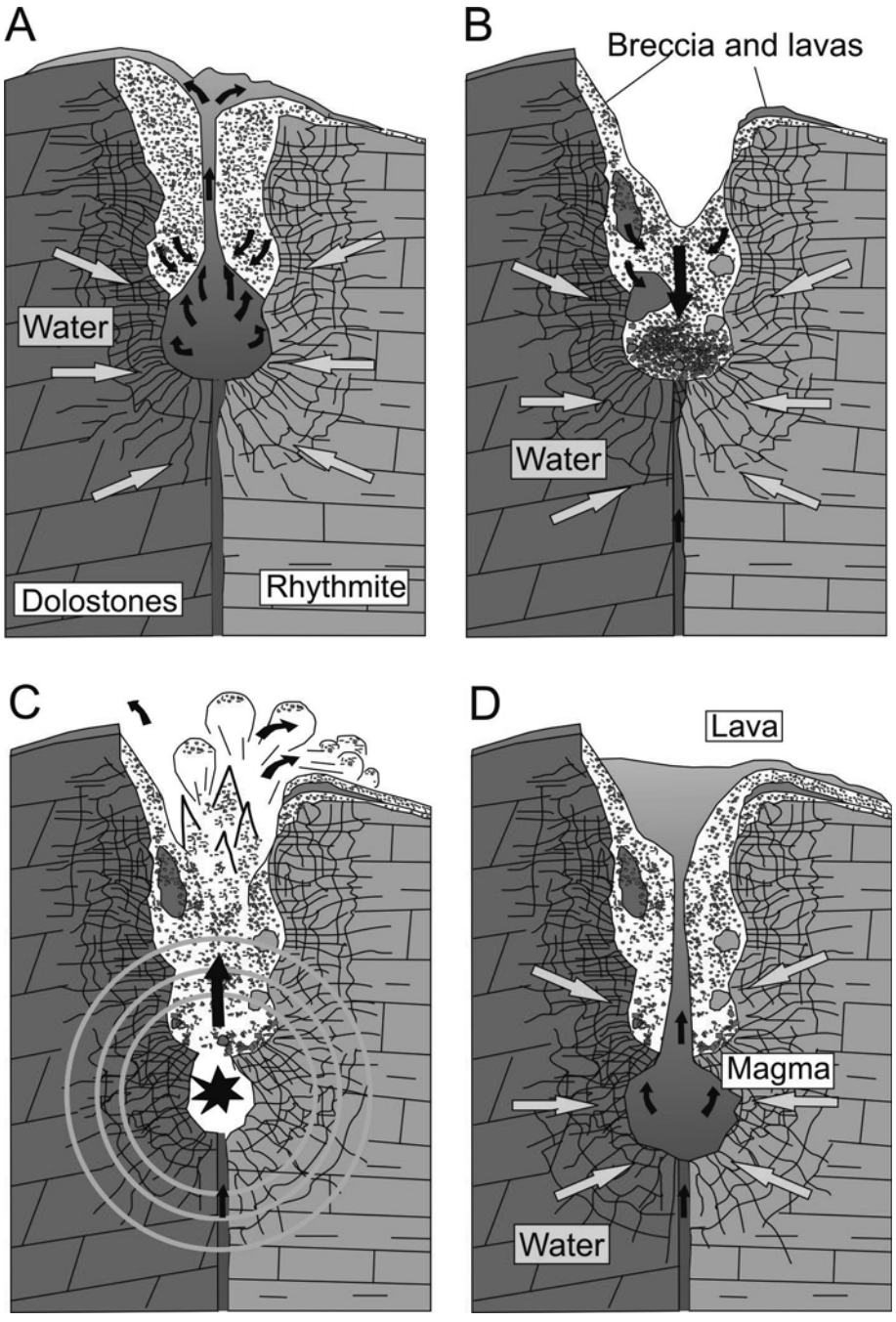

Fig. 18.- Reconstruction of the different steps during the phreatomagmatic phase of the volcanic activity: A. Eruption: magma escaping from the magmatic chamber just after the explosion. B. Collapse: chamber infilled by contact breccia and phreatomagmatic breccia. C. Explosion: the pressure in the magmatic chamber increases due to the input of magma and phreatic water, and finally produces the explosion. D: Eruption: the magma reaches the surface again after the explosion, with a wider crater and magmatic chamber.

temperatures fall and silica is introduced into the system. The texture of limestone beds within the rhythmite (mudstone to wackestone) was not affected by these alterations because of the abundance of micrite. Nevertheless, the texture of the white clasts of the phreatomagmatic breccia, completely recrystallised and featuring alteration haloes, evidences calcination. In the case of the xenoliths, especially the marly limestone xenoliths, immersed in the lava layers or even in the lamproitic body, mineralogy provides clear evidence of reaction processes favoured for higher temperatures, incorporating not only carbonates but also amphibols and K-feldspars.

Smectites are typical products of hydrothermal alteration (e.g. Clayton and Pearce, 2000; Abad *et al.*, 2003; Henry *et al.*, 2007; Jiménez-Millán *et al.*, 2008; Miyoshi *et al.*, 2013; Reolid and Abad, 2014). Saponitic smectites, characterised by a predominance of Ca in the interlayer (Table 2), were identified not only in the host rock but also in the white clasts, in the matrix of the phreatomagmatic breccia, and in the altered surface of lamproitic pyroclasts. Their presence suggests a smectite crystallisation caused by a process involving the circulation of Mg-rich fluids from the igneous rocks. The surrounding host carbonate rocks that were simultaneously altered could be a source of Ca. The textural features of the phreatomagmatic breccia, with high porosity and low cementation, facilitated the circulation of hydrothermal fluids. Indeed, the matrix of the phreatomagmatic breccia with <2 mm grain size and components from sedimentary and volcanic nature is where most mineralogical changes occurred. Saponitic smectites have been described in hydrothermal alterations of marls related to the intrusion of basalt dykes (Henry *et al.*, 2007) and the contact metamorphism of limestones affected by basic sills (Kemp *et al.*, 2005). In the Betic Cordillera, Abad *et al.* (2003) record saponite as the main phyllosilicate in the contact between the marl-limestone rhythmite and doleritic laccolith of Sierra de Priego (Córdoba), as a consequence of a late hydrothermal process after contact metamorphism produced by the intrusion of subvolcanic rocks. In this research, given the high Mg content characterising the lamproites, the record of saponite in the phreatomagmatic breccia and in the host rocks affected by the alteration processes was clearly promoted by the emplacement of the lamproitic body.

Finally, kaolinite and serpentine minerals were also found in the host rocks and in the matrix of the phreatomagmatic breccia. The presence of kaolinite in some samples of the marls closest to the phreatomagmatic breccia could indicate a fluid-mediated process under low temperatures (<200ºC) and probably favoured by post-intrusion hydrothermal fluids. Its presence is usually considered as evidence of low-temperature alteration of other aluminosilicates, especially feldspars. With regard to the serpentine minerals, their record in the matrix of the phreatomagmatic breccia, the white carbonate clasts and the xenoliths could be the result of interactions between Si and Mg-rich fluids and dolomite, as described Deer *et al.* (1992). Specifically in the case of the phreatomagmatic breccia and altered lamproitic pyroclasts, the serpentine minerals are probably the result of forsterite and enstatite alteration; in turn, vermiculite in the altered lava layers of the phreatomagmatic-effusive complex would be the result of alteration of phlogopite, but probably associated with weathering processes as described by Toksoy-Köksal *et al.* (2001).

7. Conclusions

This study was intended to characterise the phreatomagmatic phase of the eruption of the Volcano of Cancarix and the interactions between the host rocks and the lamproites. The main results may be summarised as follows:

a.- Two episodes of material emission can be distinguished: 1) explosive volcanism due to the interaction between magma and groundwater from the karstic system of the host carbonate rocks, generating a phreatomagmatic-effusive complex (breccias and lavas); and 2) emission of crystal-rich magma responsible for the main lamproitic body.

b.- The crystalline lamproitic dome of the volcano is surrounded by a ring constituted by the phreatomagmatic-effusive complex, composed by contact breccia, phreatomagmatic breccia (with pyroclast ash, lapilli and bombs, and white carbonate clasts from the host rock) and lava interlayers (massive clastogenics and banded vesiculars).

c.- The thickness and composition of the phreatomagmatic ring is conditioned by the mechanical behaviour of the country rocks. It is minimal in contact with the massive limestone-dolostones, where contact breccias predominate (Fig. 8). In contrast, phreatomagmatic deposits dominated by pyroclastic deposits are reaching a maximum thickness towards the marl-limestone rhythmites.

d.- Superimposed hydrothermal events took place in the host rocks close to the lamproites, mainly detected by textural and mineralogical changes. Porous oncolitic limestone shows the effects of circulating hydrothermal fluids up to 20 m away from the contact, with increasing contents in dolomite, amorphous silica and saponite. Yet relatively impervious marly intervals exhibit no significant mineralogical changes except for the substitution of calcite by dolomite. Limited chemical changes do occur, with enrichment in Mg, Ni, Rb, Cs, Ba, U, Th, Be, Cr, Zr and Co present in the first 8 m from the contact.

e.- Hydrothermal alteration is pervasive in the phreatomagmatic breccia —both in white carbonate clasts and matrix of the breccia— with an abundance of saponite and lizardite.

f.- Study of the phreatomagmatic complex in five detailed sections, in view of the tectonic features of the Sierra de las Cabras, led us to situate the lava conduit below the western part of the lamproite building. In this sector, contact breccia and host rock xenoliths are more common. The banded lava indicates the advance of lava in a preferently west-east direction favoured by the depressed palaeo-topography produced by the marl-limestone rhythmites.

In summary, this work reveals that spatiotemporally limited eruptions, typical of ultrapotassic magmas, are strongly

conditioned by the country rock lithology and structure. Hydrothermal processes result in a variety of low T minerals, depending on the nature of the affected rocks and the fluids from the volcano, which also impose a unique geochemical signature upon the surrounding sedimentary rocks, in turn conditioned by their permeability.

Acknowledgements

This research was supported by Projects RYC-2009-04316 (Ramón y Cajal Program, Ministerio de Ciencia e Innovación + FSE), CGL2011-30153-C02-01 (Spanish Ministry of Science and Innovation) and RNM-7408 (Junta de Andalucía), and the Research Groups RNM-325 and RNM-370 (Junta de Andalucía). We are grateful to Antonio Piedra, technician at the Laboratorio de Geología of the Universidad de Jaén, for preparation of thin sections and polished slabs. The authors thank Jean Sanders for reviewing the grammar. We also thank the *Delegación Provincial de Medio Ambiente y Desarrollo Rural de Albacete* for their authorization to work in the Monumento Natural del Pitón Volcánico de Cancarix. We are also grateful to Prof. Ioan Seghedi (Univ. Bucharest) and an anonymous reviewer for their detailed and constructive reviews.

References

Abad, I., Jiménez-Millán, J., Molina, J.M., Nieto, F., Vera, J.A. (2003): Anomalous reverse zoning of saponite and corrensite caused by contact metamorphism and hydrotermal alteration of marly rocks associated with subvolcanic bodies. *Clays and Clay Minerals* 51, 543-554. doi: 10.1346/CCMN.2003.0510508.

Aranda-Gómez, J.J., Luhr, J.F. (1996): Origin of the Joya Honda maar, San Luis de Potosí, Mexico. *Journal of Volcanology and Geothermal Research* 74, 1-18. doi: 10.1016/S0377-0273(96)00044-3.

Bishop, A.N., Abbott, G.D. (1995): Vitrinite reflectance and molecular geochemistry of Jurassic sediments: the influence of heating by Tertiary dykes (northwest Scotland). *Organic Geochemistry* 22, 165-177. doi: 10.1016/0146-6380(95)90015-2.

Bühmann, C. (1992): Smectite-to-illite conversion in a geothermally and lithologically complex Permian sedimentary sequence. *Clays and Clay Minerals* 40, 53-64. doi: 10.1346/CCMN.1992.0400107.

Clayton, T., Pearce, R.B. (2000): Alteration mineralogy of Cretaceous basalt from ODP Site 1001, Leg 165 (Caribbean Sea). *Clay Minerals* 35, 719-733. doi: 10.1180/000985500547043.

Cliff, G., Lorimer, G.W. (1975): The quantitative analysis of thin specimens. *Journal of Microscopy* 103, 203-207. doi: 10.1111/j.1365-2818.1975.tb03895.x

Contini, S., Venturelli, G., Toscani, L., Capedri, S., Barbieri, M. (1993) : Cr-Zr-armacolite-bearing lamproites of Cancarix, SE Spain. *Mineralogical Magazine* 57, 203-216. doi: 10.1180/minmag.1993.057.387.02.

Deer, W.A., Howie, R.A., Zussman, J. (1992): *An introduction to Rock-forming minerals*. Longmans Ltd., London, 696 p.

Dennis, L.W., Maciel, G.E., Hatcher, P.G., Simoneit, B.R.T. (1982): ^{13}C nuclear magnetic resonance studies of kerogen from Cretaceous black shales thermally altered by basaltic intrusions and laboratory simulations. *Geochimica et Cosmochimica Acta* 46, 901-907. doi: 10.1016/0016-7037(82)90046-1.

Duggen, S., Hoernle, K., van den Bogaard, P., Garbe-Schönberg, D. (2005): Post-collisional transition from subduction- to intraplate-type magmatism in the westernmost Mediterranean: evidence for continental-edge delamination of subcontinental lithosphere. *Journal of Petrology* 46, 1155-1201. doi: 10.1093/petrology/egi013.

Elizaga-Muñoz, E. (1994): Análisis de facies sedimentarias y petrología de los depósitos lacustres de edad neógeno superior de la Zona Prebética, Albacete, España. *Instituto de Estudios Albacetenses, Estudios Serie* 1, 74, 216 p.

Ferriz, F.J., Fernández-Soler, J.M., Cámara, F. (1994): Presencia de afloramientos de lamproitas en las proximidades de Moratalla y Cehegin (Murcia). *Boletín de la Sociedad Española de Mineralogía* 17, 231-239.

Fritschle, T., Prelević, D., Foley, F., Jacob, D.E. (2013): Petrological characterization of the mantle source of Mediterranean lamproites: Indications from major and trace elements of phlogopite. *Chemical Geology* 353, 267-279. doi: 10.1016/j.chemgeo.2012.09.006.

Fúster, J.M., Gastesi, P. (1965): Estudio petrológico de las rocas lamproíticas de Barqueros (prov. de Murcia). *Estudios Geológicos* 20, 299-314.

Fúster, J.M., Gastesi, P., Sagredo, J., Fermoso, M.L. (1967): Las rocas lamproíticas del SE de España. *Estudios Geológicos* 28, 35-69.

Grady, D.E., Kipp, M.E. (1987): Dynamic rock fragmentation. In: Atkinson, B.K. (Ed.), *Fracture Mecanics*. Academic Press, London, pp. 429-475.

Hall, A. (1987): *Igneous Petrology*. Longman Scientific and Technical, Essex. 573 p.

Henry, C., Boisson, J.-Y., Bouchet, A., Meunier, A. (2007): Thermally induced mineral and chemical transformations in calcareous mudstones around a basaltic dyke (Perthus Pass, southern Massif Central, France). Possible implications as a natural analogue of nuclear waste disposal. *Clay Minerals* 42, 213-231. doi: 10.1180/claymin.2007.042.2.07.

Hetényi, G., Taisne, B., Garel, F., Médard, E., Bosshard, S., Mattsson, H.B. (2012): Scales of columnar jointing in igneous rocks: field measurements and controlling factors. *Bulletin of Volcanology* 74, 457-482.

Jerez-Mir, L. (1973): *Geología de la Zona Prebética en la transversal de Elche de la Sierra y sectores adyacentes (provincias de Albacete y Murcia).* PhD Thesis, Univ. Granada, 749 p.

Jiménez-Millán, J., Abad, I., Nieto, F. (2008): Contasting alteration processes in hydrothermal altered dolerites from the Betic Cordillera, Spain. *Clay Minerals* 43, 267-280. doi: 10.1180/claymin.2008.043.2.09.

Kemp, S.J., Rochelle, C.A., Merriman, R.J. (2005): Back-reacted saponite in Jurassic mudstones and limestones intruded by a Tertiary sill, Isle of Skye. *Clay Minerals* 40, 263-282. doi: 10.1180/0009855054030171.

Kuiper, K.F., Krijgsman, W., Garcés, M., Wijbrans, J.R. (2006): Revised isotopic (40Ar/39Ar) age for the lamproite volcano of Cabezos Negros, Fortuna Basin (Eastern Betics, SE Spain). *Palaeogeography, Palaeoclimatology, Palaeoecology* 238, 53-63. doi: 10.1016/j.palaeo.2006.03.017.

Kurszlaukis, S., Lorenz, V. (2008): Formation of "Tuffisitic Kimberlites" by phreatomagmatic processes. *Journal of Volcanology and Geothermal Research* 174, 68-80. doi: 10.1016/j.jvolgeores.2007.12.047.

Linthout, K., Lustenhouwer, W.J. (1993): Ferrian high sanidine in a lamproite from Cancarix, Spain. *Mineralogical Magazine* 57, 289-299. doi: 10.1180/minmag.1993.057.387.11.

López-Ruiz, J., Rodríguez-Badiola, E. (1980): La región volcánica neógena del sureste de España. *Estudios Geológicos* 36, 5-63.

Lorenz, V., Kurszlaukis, S. (1997): On the last explosions of carbonatite pipe G3b, Gross Brukkaros, Namibia. *Bulletin of Volcanology* 59, 1-9. doi: 10.1007/s004450050170.

Lorenz, V., Kurszlaukis, S. (2007): Root zone processes in the phreatomagmatic pipe emplacement model and consequences for the evolution of maar-diatreme volcanoes. *Journal of Volcanology and Geo-*

thermal Research 159, 4-32. doi: 10.1016/j.jvolgeores.2006.06.019.

Lorenz, V., Zimanowski, B., Buettner, R. (2002): On the formation of deep seated subterranean peperite-like magma-sediment mixtures. *Journal of Volcanology and Geothermal Research* 114, 107-118. doi: 10.1016/S0377-0273(01)00293-1.

Mitchell, R.H., Bergman, S.C. (1991): *Petrology of lamproites*. Plenum Press, New York, 447 p.

Miyoshi, Y., Ishibashi, J.I., Faure, K., Maeto, K., Matsukura, S., Omura, A., Shimada, K., Sato, H., Sakamoto, T., Uehara, S., Chiba, H., Yamanaka, T. (2013): Mg-rich clay mineral formation associated with marine shallow-water hydrothermal activity in an arc volcanic caldera setting. *Chemical Geology* 355, 28-44. doi: 10.1016/j.chemgeo.2013.05.033.

Németh, K., Martin, U., Haller, M.J., Alric, V.I. (2007): Cenozoic diatreme field in Chubut (Argentina) as evidence of phreatomagmatic volcanism accompanied with extensive Patagonian plateau basal volcanism? *Episodes* 30, 217-223.

Niggli, P. (1923): Geinsteins und mineralprovinzen Band 1 Verlag Gebrüder: Berlin Borntraeger, 602 p.

Parga-Pondal, I. (1935): Quimismo de las manifestaciones magmáticas cenozoicas de la Península Ibérica. *Trabajos Museo Nacional Ciencias Naturales Madrid* 39, 1-174.

Pellicer, M.J. (1973): Estudio petrológico y geoquímico de un nuevo yacimiento de rocas lamproíticas situado en las proximidades de Aljorra (Murcia). *Estudios Geológicos* 29, 99-106.

Pérez-Valera, L.A., Sánchez-Gómez, M., Férnández-Sóler, J.M., Pérez-Valera, F., Azor, A. (2010): Diques de lamproítas a lo largo de la Falla de Socovos (Béticas Orientales). *Geogaceta* 48, 151-154.

Pérez-Valera, L.A., Rosenbaum, G., Sánchez-Gómez, M., Azor, A., Fernández-Soler, J.M., Pérez-Valera, F., Vasconcelos, P.M. (2013): Age distribution of lamproites along the Socovos Fault (southern Spain) and lithospheric scale tearing. *Lithos* 180-181, 252-263. doi: 10.1016/j.lithos.2013.08.016.

Prelević, D., Foley, S.F. (2007): Accretion of arc-oceanic lithospheric mantle in the Mediterranean: evidence from extremely high-Mg olivines and Cr-rich spinel inclusions in lamproites. *Earth and Planetary Science Letters* 256, 120-135. doi: 10.1016/j.epsl.2007.01.018.

Prelević, D., Foley, S.F., Romer, R., Conticelli, S. (2008): Mediterranean tertiary lamproites derived from multiple source components in postcollisional geodynamics. *Geochimica et Cosmochimica Acta* 72, 2125-2156. doi: 10.1016/j.gca.2008.01.029.

Prelević, D., Akal, C., Foley, S.F., Romer, R.L., Stracke, A., Van Den Bogaard, P. (2012): Ultrapotassic Mafic Rocks as Geochemical Proxies for Post-collisional Dynamics of Orogenic Lithospheric Mantle: the Case of Southwestern Anatolia, Turkey. *Journal of Petrology* 53, 1019-1055. doi: 10.1093/petrology/egs008.

Reolid, M., Abad, I. (2014): Glauconitic laminated crusts as a consequence of hydrothermal alteration of pillow-lavas: a microbial influence case. *Journal of Iberian Geology* 3, 389-408. doi: 10.5209/rev_JIGE.2014.v40.n3.43080.

Reolid, M., Abad, I., Sánchez-Gómez, M. (2009): Procesos tectonosedimentarios y de alteración asociados a la extrusión volcánica de Cancarix (Hellín, Provincia de Albacete). *Sabuco* 7, 11-69.

Reolid, M., Sánchez-Gómez, M., Abad, I., Gómez-Sánchez, M.E., de Mora, J. (2013): Natural Monument of the Volcano of Cancarix, Spain: a case of lamproite phreatomagmatic volcanism. *Geoheritage* 5, 35-45. doi:10.1007/s12371-012-0072-2.

Risso, C., Németh, K., Combina, A.M., Nullo, F., Drosina, M. (2008): The role of phreatomagmatism in a Plio-Pleistocene high-density scoria cone field: Llancanelo Volcanic Field (Mendoza), Argentina. *Journal of Volcanology and Geothermal Research* 169, 61-86. doi: 10.1016/j.jvolgeores.2007.08.007.

Rodríguez Estrella, T. (1979): *Geología e Hidrogeología del sector de Alcaraz-Liétor-Yeste (prov. de Albacete). Síntesis geológica de la Zona Prebética*. PhD Thesis, Univ. de Granada 1978. IGME. *Colección Memorias* 97, 566 p.

Salvioli-Mariani, E., Venturelli, G. (1996): Temperature of crystallization and evolution of the Jumilla and Cancarix lamproites (SE Spain) as suggested by melt and solid inclusions in minerals. *European Journal of Mineralogy* 8, 1027-1039.

Seghedi, I., Szakacs, A., Hernández-Pacheco, A., Brändle-Matesanz, J.L. (2007): Miocene lamproite volcanoes in south-eastern Spain: an association of phreatomagmatic and magmatic products. *Journal of Volcanology and Geothermal Research* 159, 210-224. doi: 10.1016/j.jvolgeores.2006.06.012.

Solovova, I.P., Kogarko, L.N., Ryabchikov, I.D., Naumov, V.B., Girnis, A.V., Kononkova, N.N., Venturelli, G. (1994): Spanish high-potassium magmas and evidence of their generation depth (as inferred from thermobarogeochemical data) Doklady. *Earth Science Sections* 303, 100-103.

Toksoy-Köksal, F., Türkmenoglu, A.G., Göncüoglu, M.C. (2001): Vermiculitization of phlogopite in metagabbro, Central Turkey. *Clays and Clay Minerals* 49, 81-91. doi: 10.1346/CCMN.2001.0490107.

Venturelli, G., Savioli-Mariani, E., Foley, S.F., Capedri, S., Crawford, A.J. (1988): Petrogenesis and condition of cristallization of Spanish lamproitic rocks. *Canadian Mineralogist* 26, 67-79.